

# Lawrence Berkeley National Laboratory

## LBL Publications

### Title

Diurnal Rainfall Response to the Physiological and Radiative Effects of CO<sub>2</sub> in Tropical Forests in the Energy Exascale Earth System Model v1

### Permalink

<https://escholarship.org/uc/item/7t21j2kv>

### Journal

Journal of Geophysical Research: Atmospheres, 127(10)

### ISSN

2169-897X

### Authors

Harrop, Bryce E  
Burrows, Susannah M  
Calvin, Katherine  
[et al.](#)

### Publication Date

2022-05-27

### DOI

10.1029/2021jd036148

### Copyright Information

This work is made available under the terms of a Creative Commons Attribution License, available at <https://creativecommons.org/licenses/by/4.0/>

Peer reviewed

**Key Points:**

- Physiological and radiative effects of CO<sub>2</sub> both dampen the diurnal cycle of rainfall in tropical forest regions
- Physiological effect of CO<sub>2</sub> reduces transpiration, dries boundary layer, and raises the lifting condensation level, decreasing deep convective rainfall
- Radiative effect of CO<sub>2</sub> reduces Convective Available Potential Energy leading to reductions in deep convective frequency and rainfall

**Supporting Information:**

Supporting Information may be found in the online version of this article.

**Correspondence to:**

B. E. Harrop,  
bryce.harrop@pnnl.gov

**Citation:**

Harrop, B. E., Burrows, S. M., Calvin, K., Kooperman, G. J., Leung, L. R., Maltrud, M. E., et al. (2022). Diurnal rainfall response to the physiological and radiative effects of CO<sub>2</sub> in tropical forests in the Energy Exascale Earth System Model v1. *Journal of Geophysical Research: Atmospheres*, 127, e2021JD036148. <https://doi.org/10.1029/2021JD036148>

Received 3 NOV 2021  
Accepted 23 APR 2022

© 2022. Battelle Memorial Institute. This is an open access article under the terms of the [Creative Commons Attribution-NonCommercial-NoDerivs License](#), which permits use and distribution in any medium, provided the original work is properly cited, the use is non-commercial and no modifications or adaptations are made.

## Diurnal Rainfall Response to the Physiological and Radiative Effects of CO<sub>2</sub> in Tropical Forests in the Energy Exascale Earth System Model v1

Bryce E. Harrop<sup>1</sup> , Susannah M. Burrows<sup>1</sup> , Katherine Calvin<sup>1,2</sup> , Gabriel J. Kooperman<sup>3</sup> , L. Ruby Leung<sup>1</sup> , Mathew E. Maltrud<sup>4</sup> , Xiaoying Shi<sup>5</sup> , Jinyun Tang<sup>6</sup> , Qi Tang<sup>7</sup> , Hailong Wang<sup>1</sup> , and Qing Zhu<sup>6</sup> 

<sup>1</sup>Pacific Northwest National Laboratory, Richland, WA, USA, <sup>2</sup>Pacific Northwest National Laboratory, College Park, MD, USA, <sup>3</sup>Department of Geography, University of Georgia, Athens, GA, USA, <sup>4</sup>Los Alamos National Laboratory, Los Alamos, NM, USA, <sup>5</sup>Oak Ridge National Laboratory, Oak Ridge, TN, USA, <sup>6</sup>Lawrence Berkeley National Laboratory, Berkeley, CA, USA, <sup>7</sup>Lawrence Livermore National Laboratory, Livermore, CA, USA

**Abstract** Understanding how the connection between rainfall and tropical forests will respond to increasing CO<sub>2</sub> concentrations is a key element in understanding how the tropical water cycle will respond to increasing CO<sub>2</sub>. The plant physiological and radiative impacts of CO<sub>2</sub> on rainfall patterns over tropical forest regions are examined in the Energy Exascale Earth System Model version 1.1 (E3SMv1.1-BGC) biogeochemistry experiments. Composite analysis reveals a dampening of the diurnal cycle of rainfall over the Amazon, Congo, and Maritime Continent in response to rising CO<sub>2</sub> levels, regardless of the sign of total rainfall change. A full factorial model experiment confirms that the CO<sub>2</sub> radiative and CO<sub>2</sub> plant physiological effects can individually or jointly reduce the magnitude of the rainfall diurnal cycle, though the physical pathway giving rise to the reduction differs between the two effects. For the physiological response, stomatal closure reduces evapotranspiration, which dries the boundary layer and raises the lifting condensation level. These effects combine to reduce deep convective rainfall during its peak occurrence in the late daytime to early nighttime period. For the radiative response, a relative reduction in daytime Convective Available Potential Energy (consistent with a reduction in the diurnal temperature range) leads to less frequent triggering of deep convection and a reduction of rainfall diurnal amplitude. These diurnal rainfall changes are structurally similar across seasons, and show little sensitivity to representation of nutrient coupling for the land biogeochemistry. In agreement with previous findings, the physiological response has only minor impact on extreme rainfall relative to the radiative response.

**Plain Language Summary** The distribution of rainfall in time and space is one of the key features of interest in the climate system. Simulations using the biogeochemistry-enabled version of the U.S. Department of Energy's Energy Exascale Earth System Model are used to explore how increasing atmospheric CO<sub>2</sub> concentrations impact the daily cycle of rainfall over the tropical forest regions. Increasing CO<sub>2</sub> not only warms the climate system, but also reduces the amount of transpiration from plants. These two effects are examined in isolation and are both found to reduce the daily peak in rainfall, dampening the cycle overall. The warming response is shown to make the atmosphere less favorable to convection, which reduces rainfall, while the reduced transpiration dries out the lower atmosphere, which also reduces rainfall.

### 1. Introduction

Rainfall is one of the key climate features of societal relevance (Hoegh-Guldberg et al., 2019), and is an important factor for crop growth, wildfire susceptibility, water availability, droughts, and flooding (e.g., Cloke & Pappenberger, 2009; Ozdogan et al., 2010; Vicente-Serrano et al., 2020; Westerling et al., 2003). How rainfall is distributed both in time and space often determines whether that rain is beneficial or not. As such, it is critical to better understand the physical pathways capable of altering rainfall distributions. Climate simulations are frequently used to isolate these pathways in a controlled manner. Kooperman, Chen, et al. (2018) demonstrated a robust zonal asymmetry in the tropical forest rainfall response owing to CO<sub>2</sub> increases in earth system models. Recent simulations using the biogeochemistry enabled Energy Exascale Earth System Model (E3SM; Golaz

et al., 2019; S. M. Burrows et al., 2020) v1.1 enable us to examine the impact of rising CO<sub>2</sub> on rainfall in the tropical forest regions.

Under rising atmospheric CO<sub>2</sub> concentrations, plants respond by closing their stomates to downregulate CO<sub>2</sub> gas exchange and maintain similar levels of photosynthesis, which can reduce plant transpiration (e.g., Field et al., 1995; Swann et al., 2016); hereafter referred to as the physiological effect. Swann et al. (2016) showed this stomatal closure is important in coupled simulations for mitigating the increase in evapotranspiration (ET) demand over land from the atmosphere in a warmer climate. Adams et al. (2020) have documented an observed increase in plant water-use efficiency with increasing atmospheric CO<sub>2</sub> concentration over the 20th century, but they note that the rate of increase dropped by half from the beginning to the end of the record. The stomatal closure effect on transpiration can be offset by increasing leaf area in response to rising CO<sub>2</sub>, though in dense tropical forest regions the effect is likely to be smaller than for mid-latitude forests (Kooperman, Chen, et al., 2018).

The impact this physiological effect can have on mean rainfall, particularly over the tropical forest regions, is complex. Chadwick et al. (2019) noted that the physiological effect leads to competing influences on rainfall—reductions in evapotranspiration can reduce rainfall but also leads to surface warming which can enhance rainfall. These two competing effects allow for rainfall responses of either sign over tropical land regions. Indeed, Kooperman, Chen, et al. (2018) showed that rainfall over the Maritime Continent and Congo increases while rainfall over Amazon decreases, which they linked to circulation responses between the regions. Chadwick et al. (2019) showed the land-sea temperature differences are an important factor since they exert a strong influence on the atmospheric circulation—ocean warming leads to more rainfall over ocean, less on land, while land warming leads to more rainfall over land. Chadwick et al. (2019) note, however, that the effects are nonlinear since rainfall itself can contribute to the land-sea thermal contrast. Saint-Lu et al. (2019) elaborated on those findings by showing atmospheric circulation patterns and their potential changes are important for interpreting the physiological response of rainfall to rising CO<sub>2</sub>.

The warming induced by rising CO<sub>2</sub>'s radiative impact can further complicate rainfall responses between tropical forest regions. Cook et al. (2004) showed that heating over Africa induces a Matsuno-Gill response leading to subsidence and rainfall reductions over South America. This contrast in precipitation change between Africa and South America was shown by Kooperman, Chen, et al. (2018) and Pietschnig et al. (2019) demonstrated the mechanism using idealized experiments. While this circulation response has been shown to be robust, the rainfall response over the Congo that helps drive it is still uncertain. Creese et al. (2019) examined Boreal autumn rainfall changes over the Congo in future projections in an attempt to determine which are most likely based on the physical mechanisms leading to wet and dry biases in the historical simulations. They found that models disagree on Congo basin rainfall change, but the models that dry the most tend to have the largest biases in the African Easterly Jet, suggesting they are less plausible futures. Chadwick et al. (2014) also demonstrated that the response patterns of Sea Surface Temperature warming under increasing CO<sub>2</sub> predicted by coupled models are a key component to rainfall responses, and as a result they suggest studies seeking to examine regional rainfall responses in the Tropics ought to be done with coupled atmosphere-ocean simulations.

In addition to mean rainfall changes, extreme rainfall has also been examined, though the changes owing to the physiological effect were found to be minor (Kooperman, Fowler, et al., 2018). Kooperman, Fowler, et al. (2018) showed that despite the daily rainfall extremes having minimal impact from the physiological effect, this physiological effect is a key component of extreme runoff intensity changes, accounting for roughly half of the change in 99th percentile runoff. Similarly, Fowler et al. (2019) showed that uncertainty in river flow changes, particularly extremes, comes just as much from plant responses (ET changes) as it does from rainfall responses.

Among the tropical forest regions, the Amazon has received a lot of attention for how it will respond to increasing CO<sub>2</sub> concentrations. Vilà-Guerau de Arellano et al. (2020) showed that the Amazon is a valuable environment for researching linkages between energy, moisture, and carbon fluxes and their linkage to convective development. Garcia et al. (2018) showed Amazon drought events are becoming more frequent, intense, and widespread. A recent study by Langenbrunner et al. (2019) revealed an important pathway by which the physiological response to increasing CO<sub>2</sub> leads to reduced rainfall over the Amazon. The physical pathway they identify links the reduced stomatal conductance of plants in the presence of increased CO<sub>2</sub> to a warmer, drier boundary layer, which raises the lifting condensation level (LCL) and reduces convective precipitation. They also note that these impacts occur on fast timescales without needing to invoke soil moisture changes. Of particular interest for this work was their

finding that the diurnal cycle of rainfall is impacted by the physiological response of CO<sub>2</sub>. They show a shift in rainfall to later in the day during the first several days of the experiment, but this shift transitions into a simple reduction in rainfall coinciding with the timing of its diurnal peak (their Figure 7b). This result suggests a potential dampening of the diurnal cycle of rainfall that we seek to explore in longer simulations. Reboita et al. (2016) also found a dampening of the diurnal cycle of rainfall in a regional model simulation of tropical South America with greenhouse gas warming. Their simulation, however, had no physiological CO<sub>2</sub> response, suggesting the potential for the radiative effect of increasing atmospheric CO<sub>2</sub> to act in the same manner as the physiological response.

In the present climate, the diurnal cycle of rainfall is most pronounced over land, following the pronounced diurnal cycles of solar heating and boundary layer properties that are important to convection (Dai et al., 1999; Xie et al., 2019). For general circulation models (GCMs), the precipitation diurnal cycle relies on parameterized deep convection, which is often too sensitive to surface fluxes and, as a result, consistently simulates convection too early in the day (Covey et al., 2016; Dai & Trenberth, 2004; Xie et al., 2019). Little improvement to the diurnal cycle of precipitation has been made across coupled model intercomparison project (CMIP) phases (Fiedler et al., 2020). While many studies have examined the ability of general circulation models (GCMs) to reproduce the present-day diurnal cycle, far fewer examine the response of the precipitation diurnal cycle to greenhouse gas warming. One such study, focused over North America, found an increase in diurnal rainfall intensity (Scaff et al., 2020). Another study by Meredith et al. (2021) focused on the European continent and found that diurnal cycle changes can vary across regions within Europe. Importantly, Meredith et al. (2021) used a variety of simulations including both those with and without parameterized deep convection, and while only those simulations at convection permitting resolutions were able to reproduce the observed diurnal cycle of precipitation, simulations with parameterized convection could still capture the response to warming. This result suggests that there is merit to examining the diurnal rainfall response in coarse general circulation models (GCMs), though careful scrutiny of the physical pathways giving rise to the diurnal rainfall response are needed.

There are several goals for this work that build off of the findings of Langenbrunner et al. (2019) and the previous studies outlined above. First, we test whether diurnal rainfall changes similar to those shown in Langenbrunner et al. (2019) and Reboita et al. (2016) can be found in the Energy Exascale Earth System Model (E3SM) BGC configuration across the Amazon as well as the Congo and Maritime Continent tropical forests. Second, we make use of the fact that the Energy Exascale Earth System Model (E3SM) v1.1 experiments were run with two different representations of soil nutrient limitations to examine whether the diurnal rainfall changes have any sensitivity to this particular aspect of model structural uncertainty. While Langenbrunner et al. (2019) used perpetual equinox conditions, the E3SM simulations fully resolve the seasonal cycle, and we test the sensitivity to diurnal rainfall changes across different seasons. Finally, we examine the potential implications changes in the diurnal cycle have for rainfall extremes in these tropical forest regions.

The manuscript will proceed as follows. Section 2 will outline the E3SMv1.1 model and the experiments used in this study. Section 3 will outline the changes to the diurnal cycle for the physiological effect, as well as the radiative effect and their combination. Section 4 will examine the physical pathways by which diurnal rainfall changes occur in E3SM. Finally, we will summarize the findings of this work in Section 5.

## 2. Description of Model and Experiments

Version 1 of the E3SM is described in detail by Golaz et al. (2019) and additional details pertaining to the biogeochemistry (BGC) configuration of the model are described by S. M. Burrows et al. (2020). The E3SMv1.1-BGC experiments were done with two different methods of carbon-nitrogen-phosphorous coupling: one using the Converging Trophic Cascade (CTC; P. Thornton et al., 2002; P. E. Thornton & Rosenbloom, 2005); and one using the Equilibrium Chemistry Approximation (ECA; Zhu et al., 2016; Zhu et al., 2019). The details of CTC and ECA and their implementation within the E3SM land model are outlined by S. M. Burrows et al. (2020); both configurations were shown to produce good agreement with observational benchmarks for physical and biogeochemical aspects of the land model simulation. These results can be found in the BGCv1 ILAMB data set (S. Burrows et al., 2019). Briefly, CTC uses a relative demand paradigm to resolve mineral nutrient uptake between vegetation and soil heterotrophic processes, while ECA uses a functional coupling strategy to approximate the multiple-consumer, multiple-substrate competition network. ECA simulates plant photosynthesis and leaf growth

**Table 1**  
*The Experiments Used in This Study*

Configuration	Experiment	Simulation years used in this study	Biogeochemical CO <sub>2</sub>	Radiative CO <sub>2</sub>
CTC	BCRC	2071–2100	constant	constant
	BDRC	2071–2100	diagnostic	constant
	BCRD	2071–2100	constant	diagnostic
	BDRD	2071–2100	diagnostic	diagnostic
ECA	BCRC	2071–2100	constant	constant
	BDRC	2071–2100	diagnostic	constant
	BCRD	2071–2100	constant	diagnostic
	BDRD	2071–2100	diagnostic	diagnostic

*Note.* CTC, Converging Trophic Cascade; ECA, Equilibrium Chemistry Approximation. CTC and ECA are the two biogeochemistry schemes used in the land model. Constant CO<sub>2</sub> means the values used by that component are held at constant 1,850 concentrations. Diagnostic CO<sub>2</sub> means the values are prescribed from the SSP5-8.5 scenario (O'Neill et al., 2016). The table mirrors that presented by S. M. Burrows et al. (2020, their Table 3), with the primary difference being the time periods examined.

with a flexible stoichiometry scheme and dynamic carbon allocation (Zhu et al., 2020), while CTC used fixed carbon allocation constants and fixed plant stoichiometry. Therefore, the gross primary production (GPP) and leaf area index will differ between ECA and CTC. Because plant transpiration flux is scaled with photosynthesis through stomatal controls, the difference in GPP will result in a large difference in the land surface water supply to the atmosphere between ECA and CTC. Fleischer et al. (2019) showed that phosphorous availability in models is important for the CO<sub>2</sub> fertilization effect on tropical ecosystem carbon uptake and biomass growth. They suggest that phosphorous (and other nutrients) limitation prescriptions are important to the carbon cycle, and it is worth asking whether these differences have any implication for precipitation over the tropical forest regions. In addition, phosphorous availability was not included in earlier coupled models used to assess plant responses to rising CO<sub>2</sub> (e.g., CESM1). Since the E3SMv1.1-BGC experiments include two representations of phosphorous limitation, these experiments are a good choice for examining tropical ecosystems' physiological response to rising CO<sub>2</sub> as well as the model structural uncertainty associated with the phosphorus module. The leaf stomatal conductance is computed following the Ball-Berry conductance model (Collatz et al., 1991) and is implemented following the method of Sellers et al. (1996) for GCMs. An update was made to the stomatal conductance numerical scheme to prevent negative internal leaf CO<sub>2</sub> concentrations (Golaz et al., 2019). Leaf area is predicted following the same methods as CLM4.5 (Oleson et al., 2013). E3SMv1.1-BGC uses static vegetation (S. M. Burrows et al., 2020).

As outlined by S. M. Burrows et al. (2020, their Table 3), the E3SM-BGC experiments make use of standard Coupled Climate–Carbon Cycle Model Intercomparison Project (C4MIP, Jones et al., 2016) protocols where CO<sub>2</sub> is held constant (denoted as “C”) or prescribed from a diagnostic CO<sub>2</sub> concentration based on future scenarios (denoted as “D”) for the biogeochemical and radiative impacts. We adopt the same nomenclature here where “B” refers to the physiological effect, also known as biogeochemical effect, and “R” refers to the radiative effect, and outline the experiments used in this study in Table 1. As an example, “BDRC” refers to a configuration where diagnostic CO<sub>2</sub> is used in calculating biogeochemical and biogeophysical processes, including stomatal conductance, while a constant value of CO<sub>2</sub> is used in radiative transfer calculations. The set of experiments in Table 1 allow us to compute the physiological effect as the difference BDRC – BCRC, the radiative effect as the difference BCRD – BCRC, and the full effect (the combination of the physiological and radiative effects) as the difference BDRD – BCRC. It has been shown that land cover change is a major component of changes in surface moisture, energy, and carbon exchanges (Spracklen et al., 2018). All of the experiments (BCRC, BDRC, BCRD, and BDRD) use the same SSP5-8.5 scenario (O'Neill et al., 2016) prescribed land use land cover change projection (as well as the same aerosol and non-CO<sub>2</sub> greenhouse gas concentrations) to avoid conflating land use land cover change with the CO<sub>2</sub> impacts we wish to explore. This experiment design differs somewhat from the C4MIP experiments used in previous analyses (e.g., Kooperman, Chen, et al., 2018; Kooperman, Fowler, et al., 2018; Swann et al., 2016), which were CO<sub>2</sub>-only simulations and did not include changes in land cover, aerosol, and non-CO<sub>2</sub> greenhouse gases. Thus, the radiative and physiological effects assessed from these E3SM experiments are done under more realistic conditions than the previous idealized C4MIP experiments.

The analysis period for this study is the years 2071–2100. The 2071–2100 time period is advantageous for two reasons. First, the CO<sub>2</sub> concentrations are at their largest (approximately 947 ppm) for these experiments, providing a large signal to analyze. Second, E3SMv1 has a strong aerosol sensitivity (Golaz et al., 2019), and the precipitation response to aerosol concentration changes may be similar in magnitude to that of CO<sub>2</sub> during some time periods, for example, the mid-twentieth century. We avoid the need to disentangle the aerosol changes from the CO<sub>2</sub> impacts (and their potential nonlinear interactions) by selecting the last 30 years of the SSP5-8.5 projection simulations, when anthropogenic aerosol emissions have been substantially reduced, resulting in aerosol effects that are comparatively much weaker than the CO<sub>2</sub> impact.

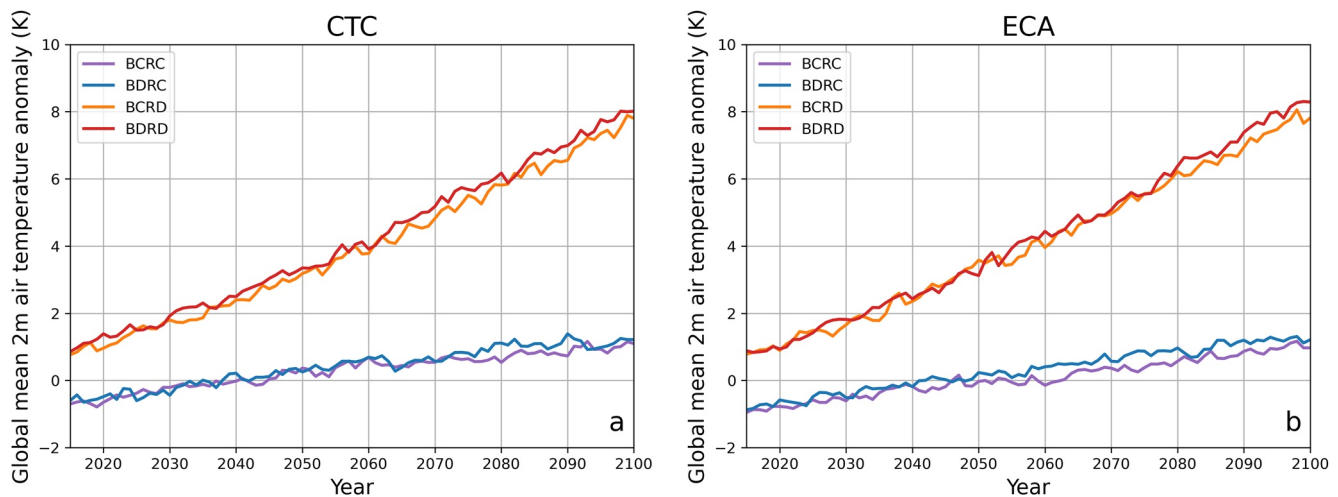


**Figure 1.** Global 2 m air temperature anomalies (relative to a 30-year average of the pre-industrial control described in (S. M. Burrows et al., 2020)) for the period 2015–2100. (a) Shows the Converging Trophic Cascade (CTC) experiments and (b) shows the Equilibrium Chemistry Approximation (ECA) experiments.

E3SMv1 has a climate sensitivity of 5.3 K (Golaz et al., 2019) which produces a warming of roughly 6–8 K relative to the pre-industrial period for the experiments with radiatively active CO<sub>2</sub> (BCRD and BDRD; see Figure 1). For the experiments with constant radiative CO<sub>2</sub> concentrations (BCRC and BDRC), there is an increase in global mean surface temperature relative to pre-industrial conditions owing to changes in aerosol, non-CO<sub>2</sub> greenhouse gases, and land use land cover change (which is prescribed to be the same for all four experiment types). As described in S. M. Burrows et al. (2020), a control simulation was also performed wherein all boundary conditions were maintained at 1,850 levels; this simulation exhibited minimal drift over 165 simulated years, indicating that changes in climate in the BCRC simulation are attributable to the changing forcings, and do not reflect an adjustment towards an equilibrium state.

For all of the analyses presented herein, we focus on the tropical forest regions of the Amazon (AMZ), Congo (CNG), and Maritime Continent (MCT). The regions are defined using the plant functional type (PFT) map used in the E3SM land model (defined using MODIS land surface mapping data; P. J. Lawrence & Chase, 2007); the basins are defined for grid cells where the tropical forest plant functional type (PFT) exceeds 70%. These basins are shown in Figure 2. The top row of Figure 2 shows the annual mean distribution of rainfall for these three regions as measured by the Tropical Rainfall Measuring Mission (TRMM, Huffman et al., 2007), and the middle and bottom rows show the biases in rainfall for the CTC and ECA configurations, respectively. Figure 2 shows that the different methods for carbon-nitrogen-phosphorous coupling have only minor impacts on the rainfall biases. The bias patterns in Figure 2 are also nearly identical to those in the non-BGC configuration of E3SM (compare with Golaz et al., 2019, their Figure 6c). The Amazon basin has too little rainfall compared to TRMM, while the Congo basin has too much rainfall relative to TRMM. The bias for the Maritime Continent forest region is less than 0.5 mm/day in magnitude, but strong positive and negative rainfall biases exist within the basin (consistent with the relative high RMSE values).

As noted above, most of the analyses in this manuscript use the time period 2071–2100, but Figure 2 presents averages over the time period of 1985–2014 to best overlap with the observed data (the TRMM data cover years 1998–2013). There are, of course, changes to the rainfall between the two 30 year periods, but the difference patterns between the model and observations shown in Figure 2 remain nearly the same in 2071–2100 (not shown). The changes in precipitation between the end of the twenty-first century and the so-called present day period (1985–2014) are presented in Table 2. Precipitation increases over the twenty-first century for the Congo and Maritime Continent basins, but decreases for the Amazon basin (except for the ECA BCRC experiment where the Amazon also has a small increase in rainfall).

Regional mean temperature increases, like the global mean, between the present day and end of twenty-first century for all regions and experiments (Table 2). As expected, those experiments with radiatively active CO<sub>2</sub> increases (BCRD and BDRD) show significantly higher increases in temperature over the twenty-first century

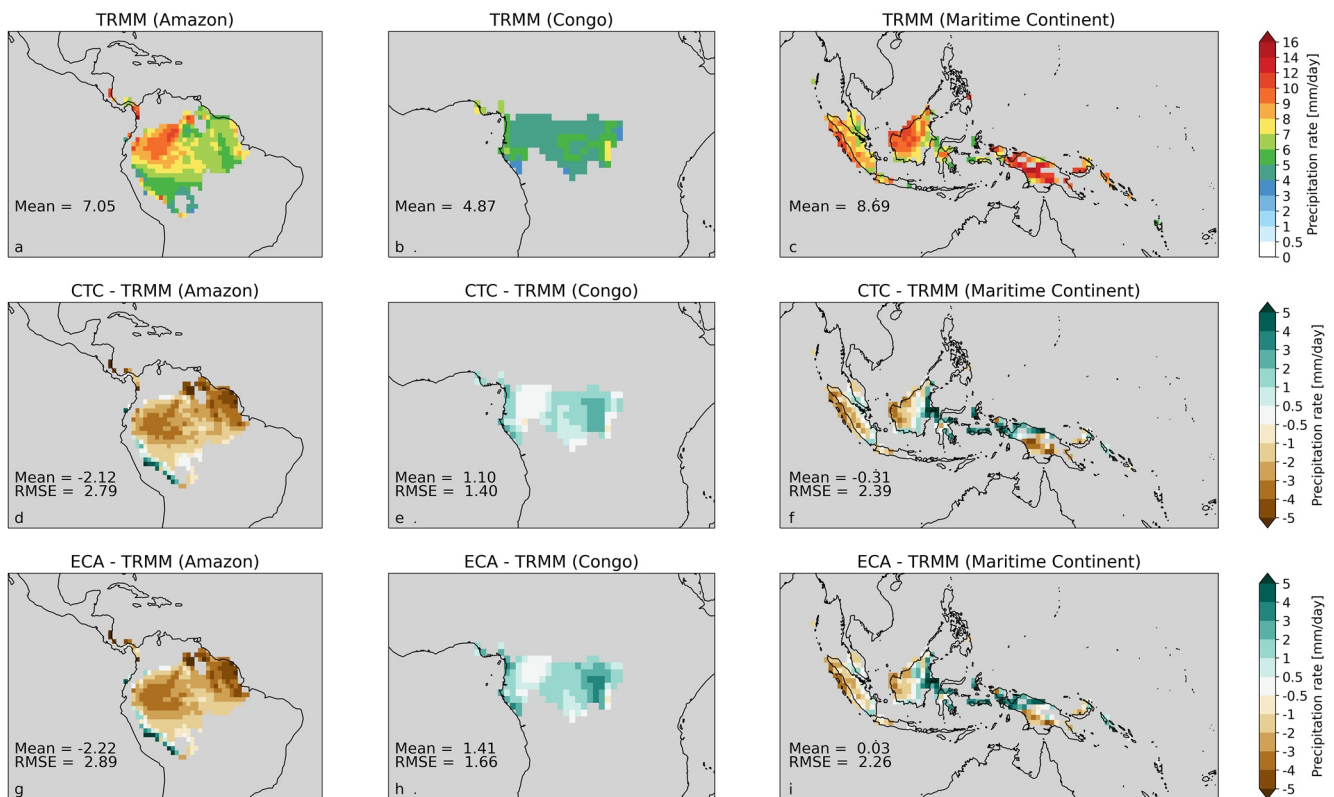


**Figure 2.** (a–c) Tropical Rainfall Measuring Mission (TRMM) annual mean rainfall, (d–f) Converging Trophic Cascade (CTC) annual mean rainfall biases, (g–i) Equilibrium Chemistry Approximation (ECA) annual mean rainfall biases, for the Amazon basin (left column), Congo basin (middle column) and Maritime Continent basin (right column). Units for all values are mm/day. Both the CTC and ECA versions of the Energy Exascale Earth System Model biogeochemistry (E3SM-BGC) model use the BDRD experiment for years 1985–2014.

than those without (BCRC and BDRC). The warming is largest for the Amazon basin and smallest for the Maritime Continent. Unlike temperature, however, the changes in rainfall are not so cleanly separated by whether  $\text{CO}_2$  is radiatively active or not. Many of the rainfall changes between 2071–2100 and 1985–2014 in the BDRD experiments are similar in magnitude to those in the BCRC and BDRD experiments. Even the BCRC experiment shows substantial changes in rainfall, particularly over the Congo. As noted above, E3SMv1 has a large aerosol sensitivity that is likely playing a non-trivial role in rainfall changes between these two time periods. For comparison purposes, we have included the values taken from the historical and SSP5-8.5 DECK five-member ensemble experiments using E3SMv1.0 (no BGC), and we show the values for both precipitation and temperature are comparable to the BCRC and BDRD experiments (note that neither BCRC nor BDRD is an exact analog for the DECK experiment).

### 3. Diurnal Rainfall Response to Rising $\text{CO}_2$

Next we examine the response of the rainfall diurnal cycle to rising  $\text{CO}_2$ . We begin by compositing 3-hourly average rainfall output into its seasonal and diurnal cycles. This is done both for the E3SM experiments (both CTC and ECA and all of BCRC, BDRC, BCRD, and BDRD) as well as the TRMM observations. Figure 3 shows these composites using BCRC, during 2071–2100, for the CTC and ECA configurations. The line plot above each panel provides the monthly mean rainfall, while the line plot to the left of each panel provides the annual mean diurnal cycle of rainfall. Overall, E3SM's simulated seasonal and diurnal cycles capture the behavior of the observed cycles of rainfall, but notable biases remain. The simulated diurnal peak tends to be early in E3SM relative to observations (which is well documented by Xie et al., 2019, and is associated with the deep convective parameterization), though this bias is larger for the Amazon (6.1/5.9 hr for CTC/ECA) and Congo (6.6/6.7 hr for

**Table 2**  
*Regional Mean Precipitation and Temperature for Present Day (PD) and the End of the Twenty-First Century (Future), as Well as Their Differences*

Experiment	PD precipitation	Future precipitation	$\Delta$ Precipitation	PD temperature	Future temperature	$\Delta$ Temperature
CTC BCRC AMZ	4.88	4.77	-0.11	297.0	298.6	1.6
CTC BCRC CNG	5.66	6.30	0.64	295.2	296.5	1.3
CTC BCRC MCT	8.38	8.66	0.28	297.3	298.4	1.1
CTC BDRC AMZ	4.96	4.69	-0.28	296.9	298.9	2.0
CTC BDRC CNG	5.79	6.36	0.57	295.2	296.8	1.6
CTC BDRC MCT	8.24	8.77	0.53	297.3	298.7	1.4
CTC BCRD AMZ	4.86	4.37	-0.49	298.0	305.3	7.3
CTC BCRD CNG	6.20	6.68	0.48	296.2	301.8	5.7
CTC BCRD MCT	8.33	8.56	0.24	298.1	303.1	4.9
CTC BDRD AMZ	4.93	4.15	-0.78	297.9	305.2	7.3
CTC BDRD CNG	5.98	6.77	0.79	296.1	302.0	5.9
CTC BDRD MCT	8.38	8.47	0.09	298.1	303.2	5.1
ECA BCRC AMZ	4.80	4.91	0.11	296.8	298.2	1.4
ECA BCRC CNG	5.90	6.50	0.60	295.4	297.1	1.8
ECA BCRC MCT	8.85	9.03	0.18	297.6	298.7	1.1
ECA BDRC AMZ	4.76	4.53	-0.23	297.0	299.0	2.1
ECA BDRC CNG	6.13	6.69	0.56	295.6	297.7	2.2
ECA BDRC MCT	8.80	9.44	0.64	297.7	299.1	1.4
ECA BCRD AMZ	4.78	4.25	-0.53	297.9	304.8	6.9
ECA BCRD CNG	6.46	6.92	0.46	296.4	302.3	5.9
ECA BCRD MCT	8.69	9.00	0.30	298.5	303.2	4.8
ECA BDRD AMZ	4.83	4.00	-0.83	298.0	305.5	7.5
ECA BDRD CNG	6.28	7.02	0.73	296.6	302.9	6.4
ECA BDRD MCT	8.73	8.86	0.14	298.6	303.7	5.1
E3SMv1.0 AMZ	4.91	4.38	-0.53	298.3	304.8	6.5
E3SMv1.0 CNG	6.90	7.36	0.46	296.7	302.4	5.7
E3SMv1.0 MCT	8.28	8.66	0.38	298.4	303.1	4.7

*Note.* AMZ, Amazon; CTC, CNG, Congo; Converging Trophic Cascade; ECA, Equilibrium Chemistry Approximation. Precipitation values are given in units of mm/day and temperature values have units of K. The PD precipitation BDRD values for CTC and ECA correspond to those shown in Figure 2 for the middle and bottom rows, respectively.

CTC/ECA) basins than for the Maritime Continent (4.7/3.6 hr for CTC/ECA) basin. The seasonality of rainfall is well captured by E3SM.

The composite difference between BDRC and BCRC (the physiological effect) is shown in Figure 4 (top row). Figure 4 removes the monthly mean to highlight the response of the diurnal cycle. The monthly mean changes can still be seen in the line plots at the top of each panel (though their differences are frequently statistically indistinguishable for individual months; not shown). The physiological effect produces a relative reduction in rainfall toward the end of the day that is largely insensitive to the season. The physiological responses for the diurnal cycle of rainfall in the ECA configuration are similar to those in the CTC configuration (see Figure S1 in Supporting Information S1). The timing of the rainfall reduction occurs near the end of the peak rainfall in E3SM (during the peak of the rainfall for TRMM observations). As such, this rainfall reduction acts to locally dampen the diurnal cycle. Note that the total rainfall goes up or down depending on the season and the nutrient coupling

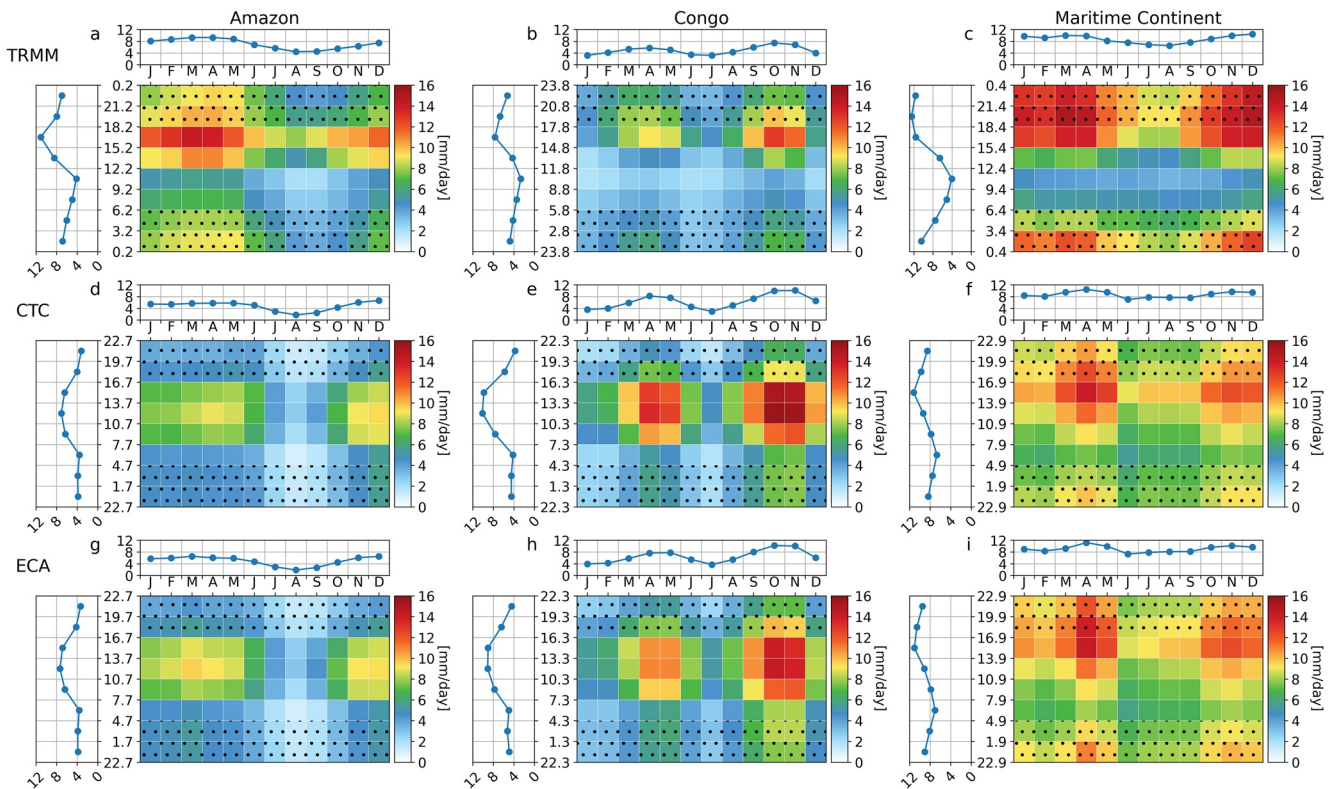


**Figure 3.** Diurnal and seasonal composite of rainfall for Tropical Rainfall Measuring Mission (TRMM) (a–c), Converging Trophic Cascade (CTC) (d–f), and Equilibrium Chemistry Approximation (ECA) (g–i), for the Amazon basin (left column), Congo basin (middle column) and Maritime Continent basin (right column). The line plots above each panel show the monthly mean seasonal cycle, and the line plots to the left of each panel show the annual mean diurnal cycle. Units for all values are mm/day. The times are given as local time based on the average longitude of each region. The Energy Exascale Earth System Model (E3SM) data and TRMM data time bounds are offset by 1.5 hr from one another. Stippling indicates nighttime. The CTC and ECA panels use the BCRC experiments for years 2071–2100. The TRMM data cover years 1998–2013.

configurations (CTC vs. ECA); it is the dampening of the diurnal cycle amplitude that is consistent across the basins, seasons, and nutrient coupling configurations.

The composite difference between BCRD and BCRC (the radiative effect) is shown in Figure 4 (middle row). Like for the physiological effect, there is a dampening of the diurnal cycle of rainfall owing to the radiative effect. Even after removing the monthly means, it is apparent that there is some variation in the timing of the rainfall reduction, most notably for the Congo basin. Unlike the physiological effect, changes in the seasonal cycle of rainfall owing to the radiative effect are consistent between the CTC and ECA configurations (compare Figures 4 and S1 in Supporting Information S1). Over the Amazon and Maritime Continent, the rainfall reduction is most prominent during the end of the dry season and wet season initiation period, consistent with a delay in the seasonal cycle of the Intertropical Convergence Zone progression found in models and observations, which is most robust over land (Song et al., 2018a, 2018b, 2021). For the Congo, the rainfall reduction is largest during the wet seasons.

The full effect (BDRD – BCRC) has a similar reduction pattern in diurnal rainfall amplitude to the physiological and radiative effects (Figure 4 bottom row). The magnitude of the full effect is similar to the sum of the physiological and radiative effects. It is remarkable that the diurnal amplitude response is qualitatively similar for both the physiological and radiative effects of increasing atmospheric CO<sub>2</sub> concentrations. Quantitatively, the reduction in precipitation during the day is larger for the radiative effect than the physiological effect, as we will show later, potentially resulting from the large equilibrium climate sensitivity in E3SMv1 (Golaz et al., 2019). To better understand this reduction in rainfall diurnal cycle amplitude, we examine the moisture budget.

$$\frac{\partial w}{\partial t} + \nabla \cdot \int_0^{p_{\text{sfic}}} \mathbf{v}q \, dp = E - P \quad (1)$$

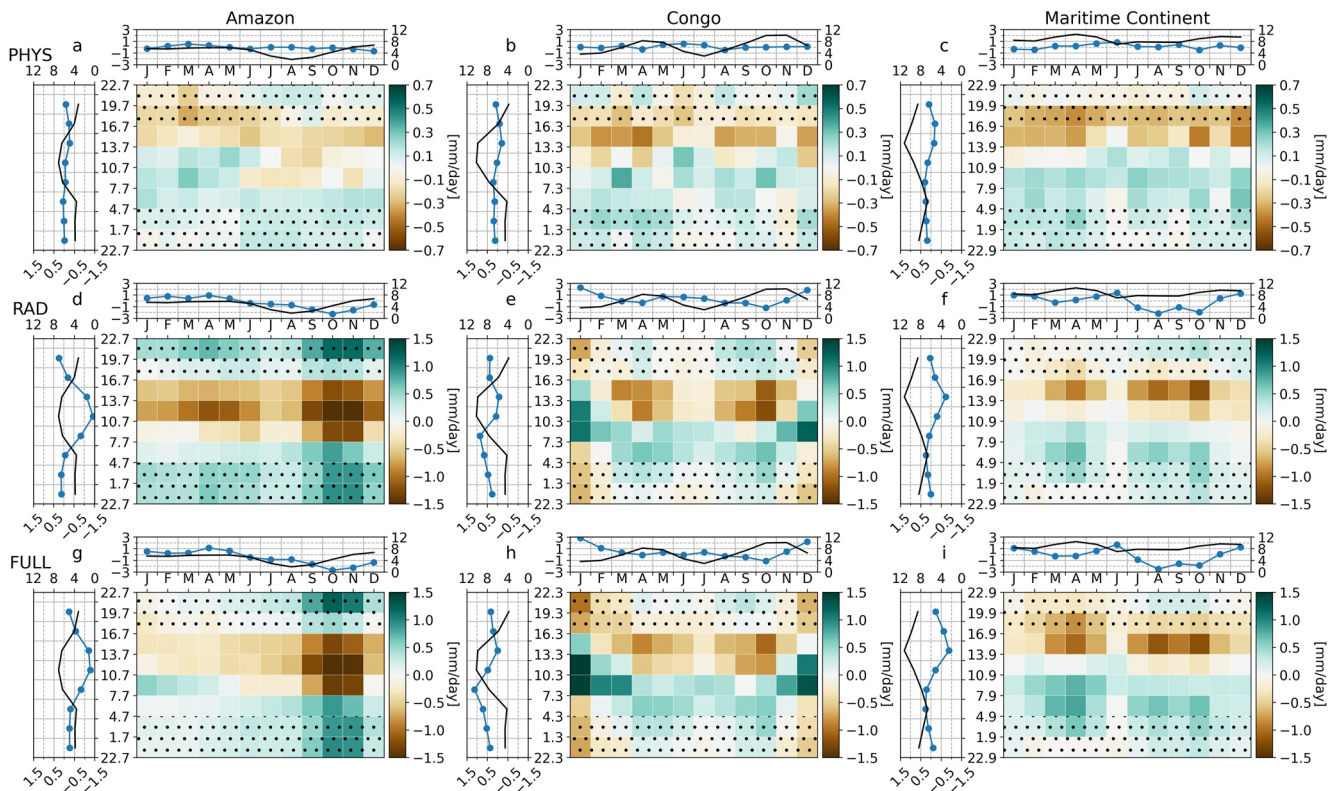


**Figure 4.** As in Figure 3, but for the physiological effect (BDRC – BCRC; top row), radiative effect (BCRD – BCRC; middle row), and full effect (BDRD – BCRC; bottom row) for the Converging Trophic Cascade configuration. Monthly mean differences have been removed from the colored difference panels, but are shown in the line plots above each panel. The annual mean diurnal response shown in the line plot to the left of each panel does not have the monthly means removed (and thus may differ in magnitude relative to the colored panels). In the line plots above and to the left of each panel, the blue line with circle markers denotes the differences (values on bottom or left axis) and the black line with no marker denotes the baseline (BCRC; values on top or right axis). All values are in units of mm/day.

where  $w$  is the precipitable water,  $q$  is the specific humidity,  $\mathbf{v}$  is the horizontal wind vector,  $p$  is the pressure,  $g$  is the gravitational acceleration constant,  $E$  is the surface evapotranspiration (ET), and  $P$  is the surface precipitation. From Equation 1, we can get the changes in precipitation as the sum of three terms:

$$\Delta P = \Delta E - \Delta \left( \frac{\partial w}{\partial t} \right) - \Delta \left( \nabla \cdot \int_0^{p_{\text{sc}}} \mathbf{v} q \frac{dp}{g} \right) \quad (2)$$

the change in surface ET, the change in atmospheric moisture storage, and the change in atmospheric moisture convergence. The contributions to rainfall changes are shown in Figure 5 for the physiological, radiative, and full effects (top, middle, and bottom rows, respectively). The small residuals in the moisture budget confirm the suitability of this approach for the model output.

The physiological effect shows a large reduction in ET between roughly 7:00–17:00 local time across the three basins (see Figure 5 top row). This result is consistent with stomatal closure reducing transpiration during the day (there is little transpiration at night even for BCRC) under higher atmospheric  $\text{CO}_2$  concentrations. The decline in ET is larger in ECA than CTC (compare Figure 5 with Figure S2 in Supporting Information S1), though the differences vary from region to region with the Amazon having the largest difference and the Congo having the smallest. While there are some changes to moisture convergence (e.g., large increase in moisture convergence over the Maritime Continent), the diurnal variations in moisture convergence changes are generally smaller than those from the other terms. The storage term largely acts to offset the changes from the other terms, which for the physiological effect, amplifies the diurnal cycle of rainfall. Of course, on these 3-hourly timescales, changes in ET or convergence are not guaranteed to instantaneously result in precipitation, and the storage term will reflect any delay (e.g., associated with reduced convective triggering). Another way to conceptualize the storage term is that it encompasses physical processes like vertical mixing that link surface fluxes and moisture

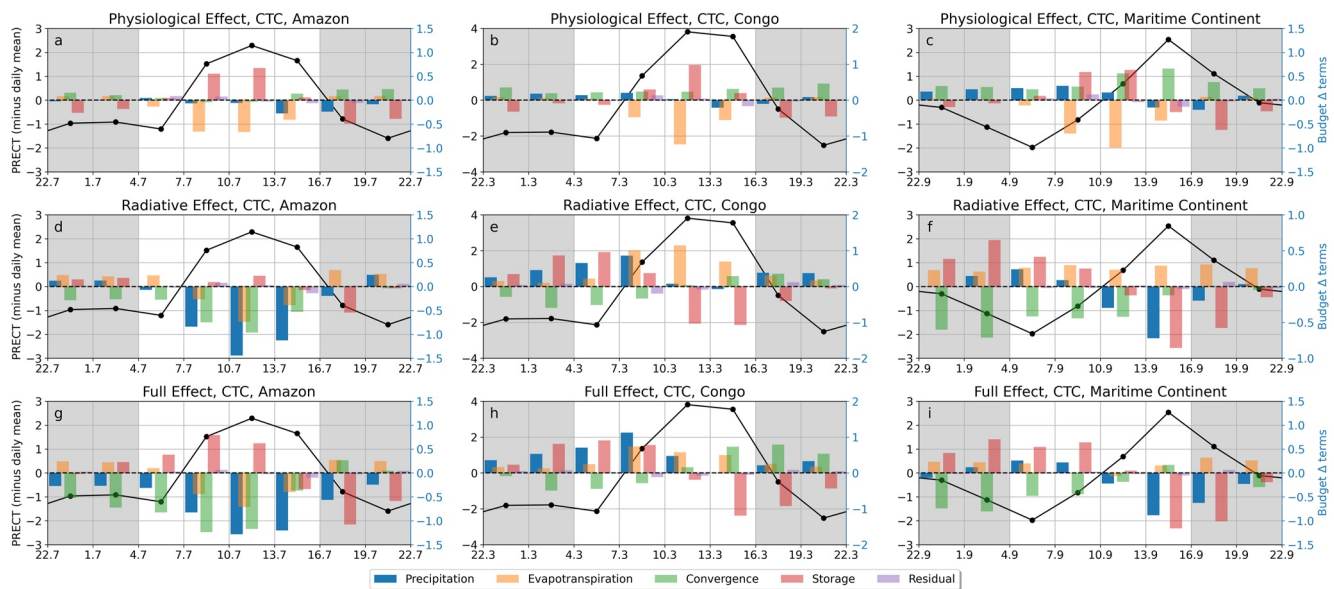


**Figure 5.** Diurnal cycle of rainfall (black line) with daily mean removed for BCRC (CTC configuration). The changes in precipitation (blue), evapotranspiration (orange), moisture convergence (green), storage (red), and the residual (purple) are shown as bars. The abscissa is local time and the gray shading denotes nighttime. The left ordinate axis is the diurnal variations in BCRC and the right ordinate axis is the magnitude of the budget terms. The top row shows the physiological effect (BDRC – BCRC), the middle row shows the radiative effect (BCRD – BCRC), and the bottom row shows the full effect (BDRD – BCRC). The left column shows the Amazon basin, the middle column shows the Congo basin, and the right column shows the Maritime Continent basin. All values are given in units of mm/day. The ordinate axes limits vary between panels.

convergence to rain formation. We explore these physical pathways in more detail in Section 4. For the present discussion, this budget framework provides a sense of the basic components most important for the dampening of the diurnal rainfall signal, which for the physiological effect is the surface ET.

Figure 5 (middle row) shows the moisture budget terms for the radiative effect. Unlike the physiological response, surface ET does not consistently decrease across all basins. Only the Amazon shows a decline in ET owing to the radiative warming from CO<sub>2</sub> (we show in Section 4 that this stems from reduced leaf area index). The Congo and Maritime Continent show increases in ET. While the physiological effect generally showed increasing moisture convergence across the basins, the radiative effect shows decreases in moisture convergence across the tropical forest regions. With respect to dampening the rainfall diurnal cycle amplitude, it is the storage term that has the largest contribution, except over the Amazon basin where surface ET and moisture convergence are responsible for the amplitude reduction.

Figure 6 provides a summary table of the diurnal cycle amplitude changes for each of the moisture budget terms separated into the physiological (PHYS; BDRC – BCRC), radiative (RAD; BCRD – BCRC), and full (FULL; BDRD – BCRC) effects. The amplitudes are computed using circular statistical mean (which is equivalent to the first mode in a discrete Fourier Transform) relative to the annual total as in Markham (1970). The amplitude changes attributed to each term are constructed by adding the change in precipitation related to that term to the baseline (BCRC) precipitation and computing the amplitude of the resulting diurnal cycle. Each year within the 30-year time period is treated as an independent sample in a *t*-test statistic to determine significance of the changes. Values in Figure 6 that are colored are statistically significant at the 95th percentile.

The values in Figure 6 use the full annual cycle. Additional tests were done using the six wettest months (as a proxy for the wet season) and the six driest months (as a proxy for the dry season). For the Amazon, the wet season is December through May; for the Congo, the wet season is March through May and September through November; and for the Maritime Continent, the wet season is November through April. There is little seasonal variation in the physiological response, but the radiative response is sensitive to the time of year the values are computed over (Figures S3 and S4 in Supporting Information S1). The Amazon basin, in particular, shows a

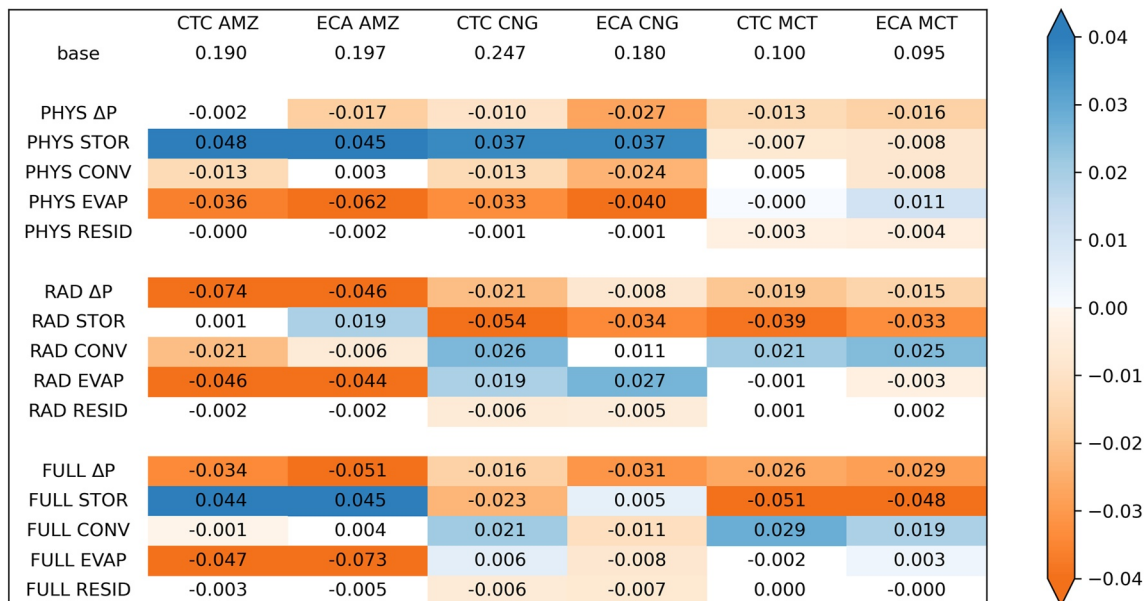


**Figure 6.** Summary of amplitude changes for each term in the moisture budget separated into the physiological (PHYS; BDRD – BCRC) effect, radiative (RAD; BCRD – BCRC) effect, and full (FULL; BDRD – BCRC) effect. Values that are colored are statistically significant at the 95th percentile. Orange colors are those where the diurnal amplitude is dampening and blue colors denote an amplifying change.

strong sensitivity to the wet and dry periods. During the wet period, it is the storage and convergence terms that dominate the radiative dampening of the diurnal cycle. During the dry period, however, the dampening over the Amazon occurs via changes in ET. The annual mean response resembles the dry period more than the wet period. The full effect resembles a combination of the physiological and radiative effects for the annual mean, wet season, and dry season (the qualitative pattern is the same between the full effect and the linear combination of the physiological and radiative effects, not shown).

In addition to examining the amplitude response to increasing CO<sub>2</sub>, we examined the phase response of the diurnal cycle (Figure 7). While many of the phase changes are statistically significant at the 95th percentile, the magnitude of the phase changes are all less than three hours. Given that this is the frequency of the model output, it is difficult to robustly interpret these phase changes, so we leave examination of any potential phase changes to future research efforts. We report our findings for the phase changes in Figure 7 to encourage comparison for those future efforts. Additionally, there is one feature in Figure 7 that is of interest to this work: the phase delay owing to changing ET physiological response. The delay, while small, is consistent across all regions for both CTC and ECA. We will discuss this in more detail in Section 4.

It is important to recognize the limitations of the above moisture budget analysis for explaining the dampening of the diurnal rainfall pattern. The attribution of the rainfall changes to the various terms relies on their alignment in time. By construction, the amplitude metrics shown in Figure 6 are maximized where processes overlap with the peak in diurnal rainfall. Any phase shifts between a process and its rainfall response that exceed the 3 hour sampling frequency have the potential to be mischaracterized by that metric. For example, the precipitation phase bias is smaller for the Maritime Continent than for the Amazon and Congo basins, meaning the peak precipitation does not align as closely with the reduction in evapotranspiration. The Maritime Continent is also the only basin among the three that does not show a decrease in rainfall diurnal amplitude for the physiological response in Figure 6. It is worth asking whether these differences are an artifact of this analysis method or if there are important physical differences between these regions. Thus, it is important to examine the physical pathways governing the response of E3SM to rising CO<sub>2</sub> concentrations. These physical pathways are described in the following section.

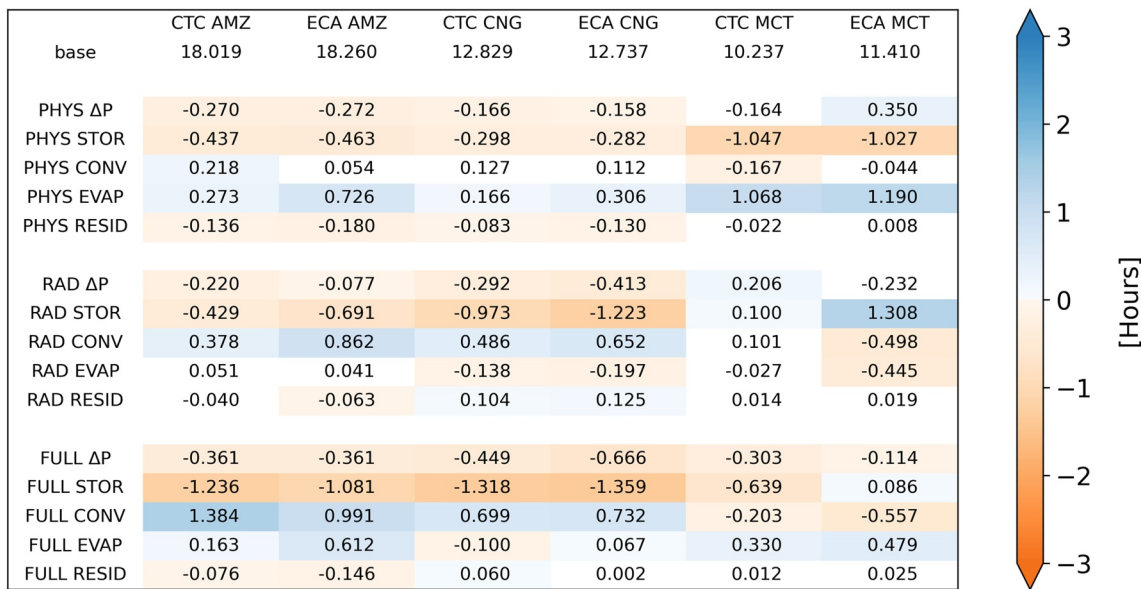


Figure 7. Same as Figure 6, only for the diurnal phase of rainfall. Units are in hours.

#### 4. Physical Pathways Responsible for CO<sub>2</sub> Impacts

In order to examine the physical pathways giving rise to the dampened diurnal cycle of rainfall shown in Section 3, additional 3-hourly model output was needed that wasn't available from the initial simulation campaign. Figures 4–6 reveal that the CTC and ECA configurations have the same physiological and radiative responses to increasing CO<sub>2</sub>, suggesting that the physical pathways that dominate the dampening of the rainfall diurnal cycle are robust across different BGC representations. As a result, and to save on computational demands, 10 year segments (2071–2080) of the CTC configuration BCRC, BDRC, BCRD, and BDRD experiments were rerun with additional atmosphere and land model fields (a list of the additional fields used in this study can be found in Appendix A). These 10 year segments reproduce the general characteristics of Figures 3–6 (not shown). For the analyses in this section, unless noted otherwise, the results make use of these 10 year segments.

The first aspect of the reruns is an examination of the evapotranspiration term separated into its components. For the E3SM Land Model (ELM), there are three terms that sum to the total evapotranspiration: transpiration, soil evaporation, and canopy evaporation (as in its predecessor model the Community Land Model; D. M. Lawrence et al., 2007). Figure 8 shows the changes to the total ET as well as its terms for the physiological (second row), radiative (third row), and full (bottom row) effects. The ratio of transpiration to ET ranges between 62% and 65% across the Amazon, Congo, and Maritime Continent. These values are nearly identical to the global average estimate of 62% ± 6% (Lian et al., 2018), though Figure 1a of Lian et al. (2018) suggests those values may be a slight underestimate for the tropical forests. Additional comparisons were made as part of the overview analysis of the E3SMv1.1 experiments by S. M. Burrows et al. (2020) using the International Land Model Benchmarking (ILAMB; Collier et al., 2018) system. Evaporative fraction biases over the tropical forests are small compared to Global Bio-Atmosphere Flux (GBAF; Jung et al., 2010) for both CTC and ECA. ET compares well to remote sensing derived estimates from the Moderate Resolution Imaging Spectroradiometer (MODIS; De Kauwe et al., 2011) over these regions, but less well relative to Global Land surface Evaporation: the Amsterdam Methodology (GLEAM; Miralles et al., 2011), which suggests that E3SMv1.1 does a suitable job at reproducing the annual mean observed ET and evaporative fraction.

Unsurprisingly, the physiological effect is dominated by changes in transpiration (Figure 8 second row). The stomatal closure in the presence of increased atmospheric CO<sub>2</sub> concentrations reduces transpiration over all three tropical forest regions. The reduced ET in the physiological experiments during the day is compensated by increased sensible heat flux (not shown) which gives rise to the increasing daytime 2 m air temperatures shown in the gray curves. Note that an exact correspondence between ET and temperature is not expected since

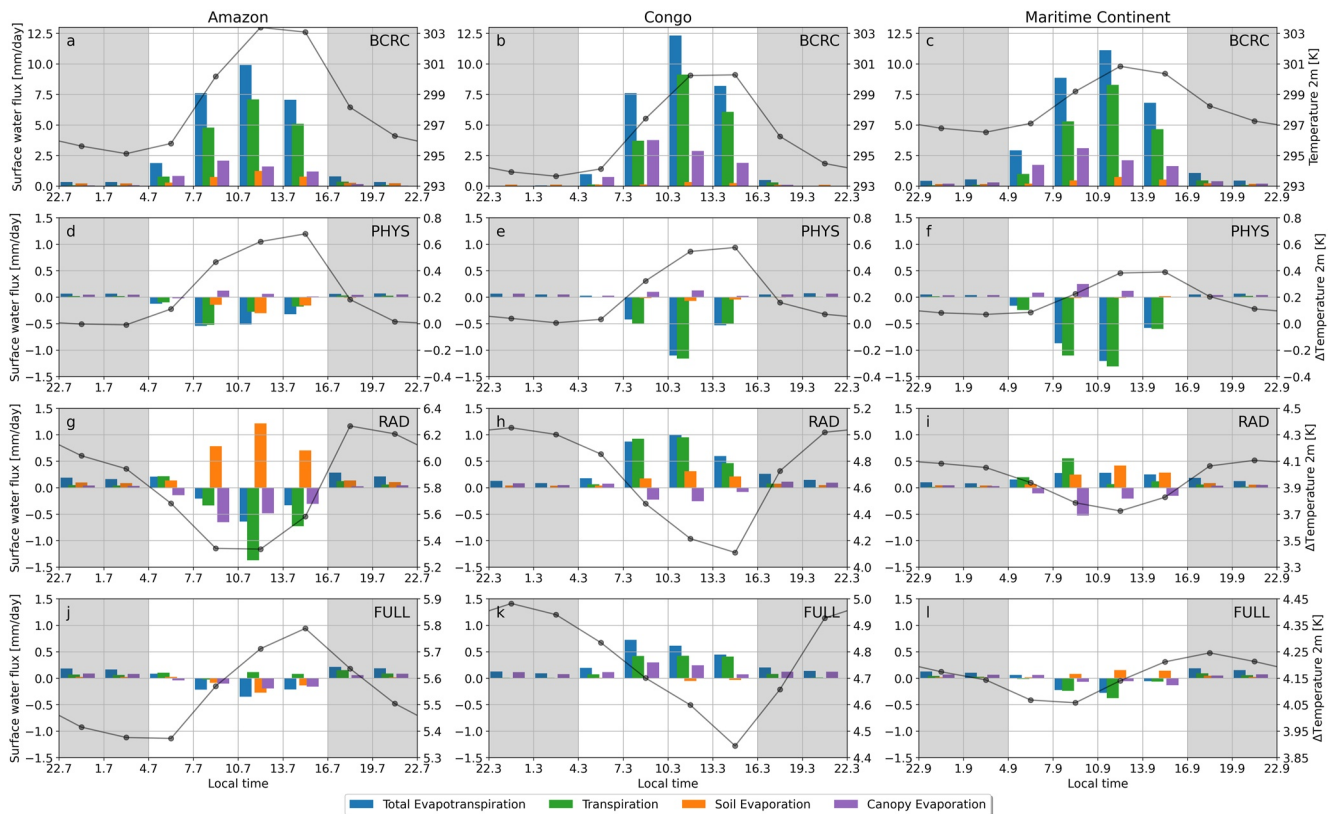


**Figure 8.** Diurnal cycle of evapotranspiration (BCRC; top row) and its changes owing to the physiological effect (BDRC – BCRC; second row), radiative effect (BCRD – BCRC; third row), and full effect (BDRD – BCRC; bottom row) for the Amazon (left column), Congo (middle column), and Maritime Continent (right column). The blue bars represent the total evapotranspiration, the green bars represent transpiration, the orange bars represent soil evaporation, and the purple bars represent canopy evaporation. Like Figure 5, the gray shading indicates local nighttime. All bar values are given in units of mm/day. The gray lines are the 2 m air temperature (BCRC; top row) and 2 m air temperature difference owing to the physiological effect (BDRC – BCRC; second row), radiative effect (BCRD – BCRC; third row), and full effect (BDRD – BCRC; bottom row). All temperature values are in units of K.

temperature is subject to other effects such as mixing in the boundary layer. The radiative and full effects are more complicated, particularly over the Amazon basin (bottom two rows of Figure 8). There is a significant reduction in leaf area in the radiative response (Figure 9) which decreases both transpiration and canopy evaporation, while increasing soil evaporation. All else equal, an increase in leaf area index is expected to increase transpiration at

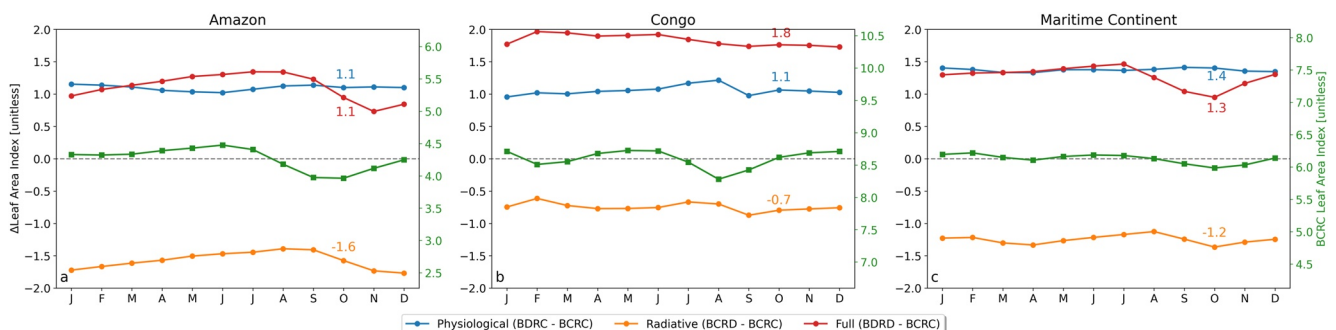


**Figure 9.** Seasonal cycle of leaf area index change (unitless) for the physiological (BDRC – BCRC; blue), radiative (BCRD – BCRC; orange), and full (BDRD – BCRC; red) experiments. Panel a is for the Amazon, panel b is for the Congo, and panel c is for the Maritime Continent region. There is no diurnal variability in the leaf area index. The values of the annual mean leaf area index differences are provided in each figure with the color differentiation the same for the text and lines. The green line and axis denotes the baseline (BCRC) experiment leaf area index. The axes for the baseline are scaled so the magnitude of the changes is comparable to the seasonal cycle.

the expense of soil evaporation. The increase in leaf area for BDRC relative to BCRC confirms that it is not a change in leaf area driving the decrease in transpiration between these experiments. The overall effect is still a decrease in total ET, but only as a result of large offsetting changes in its component terms. The full effect does not exhibit the same decrease in leaf area with increasing temperatures like the radiative effect, but instead sees an increase in leaf area similar to the BDRC experiment (their annual mean changes are virtually identical as shown in Figure 9a). In other words, the reduction in leaf area with warming is not present in E3SM when the plants are allowed to respond to the elevated CO<sub>2</sub> concentrations directly. Even though the stomatal closure and leaf area increases are similar between the physiological and full effects, the transpiration actually increases for the full effect. We speculate that this may be related to higher evaporative demand from a warmer atmosphere (there is a decrease in near surface relative humidity over the Amazon; not shown) outweighing increases in the plants' water use efficiency, but a careful examination of the plant response is beyond the scope of this effort. Follow up work is needed for better understanding the plants' response to warming with/without CO<sub>2</sub> increases (e.g., LAI changes in BDRD vs. BCRD) and the impacts on transpiration caused by these changes.

The Amazon is the only region where the full effect of transpiration is not simply a balance between the physiological and radiative effects. It is also the only tropical forest region where the radiative effect sees large reductions in transpiration. The Congo and Maritime Continent basins both show increases in transpiration owing to the radiative effect. The increase in transpiration is small for the Maritime Continent and largely offset by decreases in canopy evaporation. Over the Congo, the increases in transpiration drive increases in ET which accounts for the amplifying diurnal rainfall signal for the RAD EVAP term in Figure 6. For the Congo basin, the radiative effect dominates and the ET increases with CO<sub>2</sub>, but for the Maritime Continent, the physiological effect dominates and ET decreases with rising CO<sub>2</sub>.

In our moisture budget analysis above, the surface ET flux changes dominate the physiological rainfall diurnal cycle response only for the Amazon and Congo basins. Figure 8, however, shows that surface ET decreases for all three basins and that it is driven by transpiration changes. A natural follow up question is, how do these changes in transpiration lead to a reduction in the rainfall amplitude over these tropical forest basins? To answer this question, it is important to know how rainfall is generated in the model. In E3SM, rainfall is generated by both resolved and parameterized vertical moisture transport. The deep convection parameterization, which is treated separately from shallow convection, macrophysics, and microphysics, is responsible for the majority of tropical precipitation formation, including the three tropical forest regions (between 75% and 82% of total rainfall comes from the deep convective parameterization for these regions in the BCRC experiment; not shown). For reference, the deep convective parameterization used in E3SM is based on the formulation described by Zhang and McFarlane (1995) with additional modifications by Neale et al. (2008) and Richter and Rasch (2008). This deep convective scheme calculates cloud base mass flux using a closure designed to reduce Convective Available Potential Energy (CAPE) with a prescribed timescale (3,600 s for these simulations). In other words, parameterized deep convection is formulated to respond directly to changes in Convective Available Potential Energy (CAPE). Additional details on the deep convective and other atmospheric parameterizations are detailed by Rasch et al. (2019). Like the baseline rainfall, changes in rainfall for the tropical forest regions also occur primarily as the result of changes in deep convective rainfall (not shown). Therefore, to understand the sensitivity of rainfall to reduced transpiration, we need to understand the sensitivity of the deep convective parameterization to reduced transpiration, and, as will be shown later, how Convective Available Potential Energy (CAPE) responds to reduced transpiration.

Figure 10 shows the annual mean diurnal cycle of the vertically resolved water vapor tendency from the deep convective parameterization. The black contours provide the baseline values from the BCRC experiment, and the color-filled contours show the response coming from the physiological (BDRC – BCRC; top row), radiative (BCRD – BCRC; middle row), and full (BDRD – BCRC; bottom row) effects. Negative tendencies (dashed, black contours) are where water vapor is condensed and rained out of the atmosphere by the deep convective parameterization. Consistent with the above figures, the dashed contours are concentrated during the daytime and have their largest values toward the end of the day. Red-filled contours show an increase in the deep convective water vapor tendency. Where red contours overlap dashed contours, there is less condensation occurring in the experiment relative to BCRC, which implies a reduction in the rain formed by the deep convective parameterization.

Figure 10 shows the dampening of the rainfall diurnal cycle by the physiological effect results from a reduction in condensation in the lower atmosphere (between 800 hPa and the surface). There is an increase in condensation

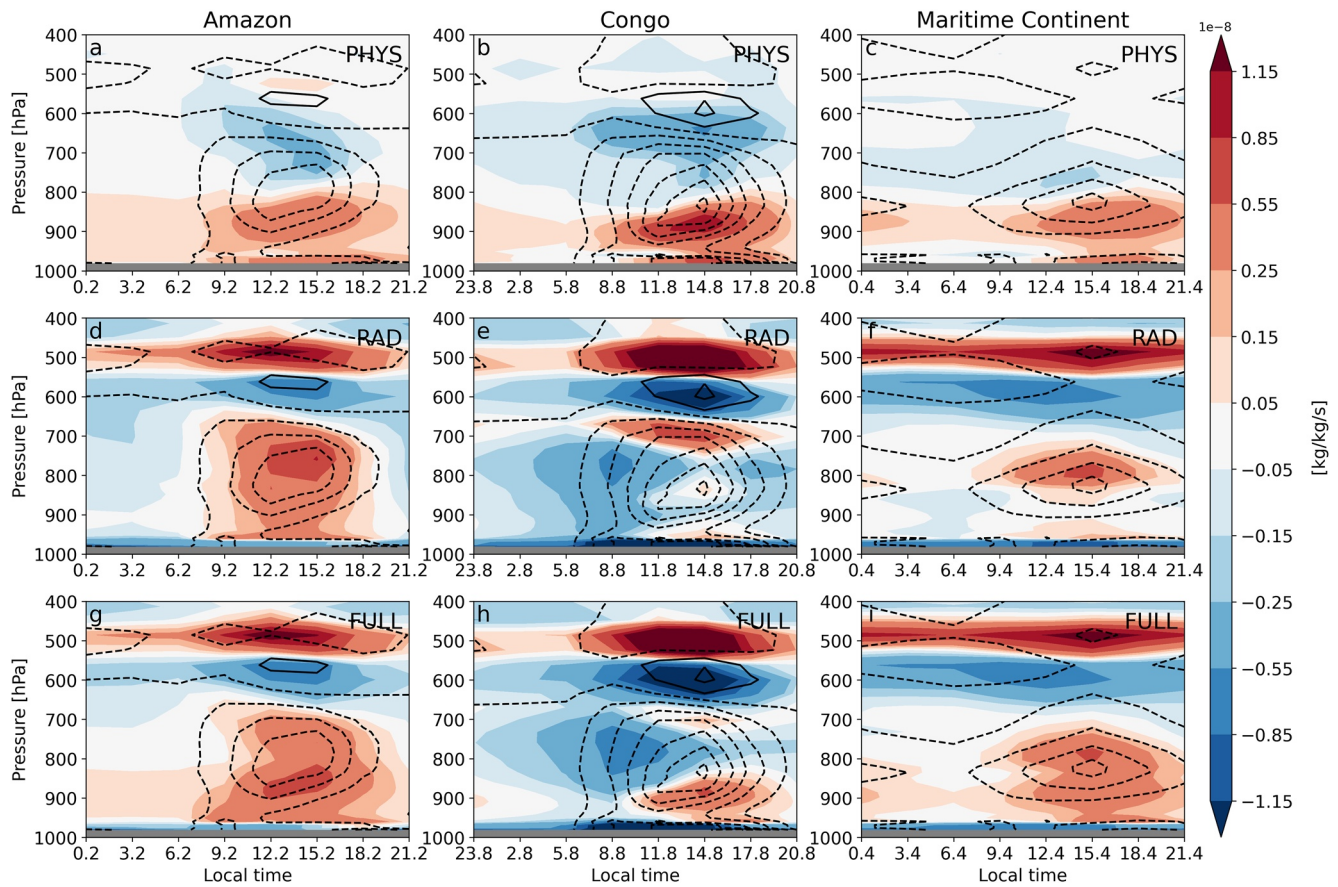


**Figure 10.** Deep convective water vapor tendency for the BCRC experiments (black contours) and its change (color-filled contours) with respect to the physiological effect (BDRC – BCRC; top row), radiative effect (BCRD – BCRC; middle row), and full effect (BDRD – BCRC; bottom row) for the Amazon (left column), Congo (middle column), and Maritime Continent (right column). The black contours have an interval of  $1 \times 10^{-8}$  kg/kg/s. Solid/red contours denote positive values and negative/blue contours, dashed. Red-filled contours denote pressure levels at the local time where less deep convective condensation occurs in the experiment relative to BCRC. In other words, less rainfall is generated from the deep convective parameterization in experiments where contours are red. The gray region denotes pressure levels exceeding the annual mean surface pressure for the region.

above this level, but not enough to offset the reduction such that the total rainfall is reduced. The reduction in condensation at lower levels suggests that the reduction in surface ET via stomatal reducing of the transpiration is raising the lifting condensation level (LCL) and causing condensation to begin at higher levels in the perturbed climate (BDRD) relative to the baseline (BCRC). This relationship is confirmed by computing the lifting condensation level (LCL) for each experiment and over each region. The lifting condensation level (LCL) height is computed by first calculating its temperature following Equation 21 of Bolton (1980), then using the dry adiabatic lapse rate together with the surface altitude and temperature to find the altitude where the LCL temperature occurs.

Figure 11 shows that there is a significant increase in LCL height for the physiological response to increasing  $\text{CO}_2$ . As expected with an increased LCL, cloud base is similarly elevated (not shown). Additionally, these LCL increases occur at the same times as the reduction in rainfall seen in Figure 4. Furthermore, the timing of the LCL changes are consistent between the physiological and full effects (second and fourth rows of Figure 11). Taking together the change in LCL, deep convective water vapor tendency, transpiration, and increased near surface temperature, we can explain the rainfall amplitude reduction simply as the atmosphere's response to a drier and warmer boundary layer leading to elevated cloud base and less vapor available for condensation. This mechanism is in agreement with the results of Langenbrunner et al. (2019), lending additional confidence to our conclusion. The reduction in the diurnal cycle amplitude occurs primarily because the deep convective parameterization is most active during the day when the transpiration peaks. Precipitation peaks somewhat later over the Maritime

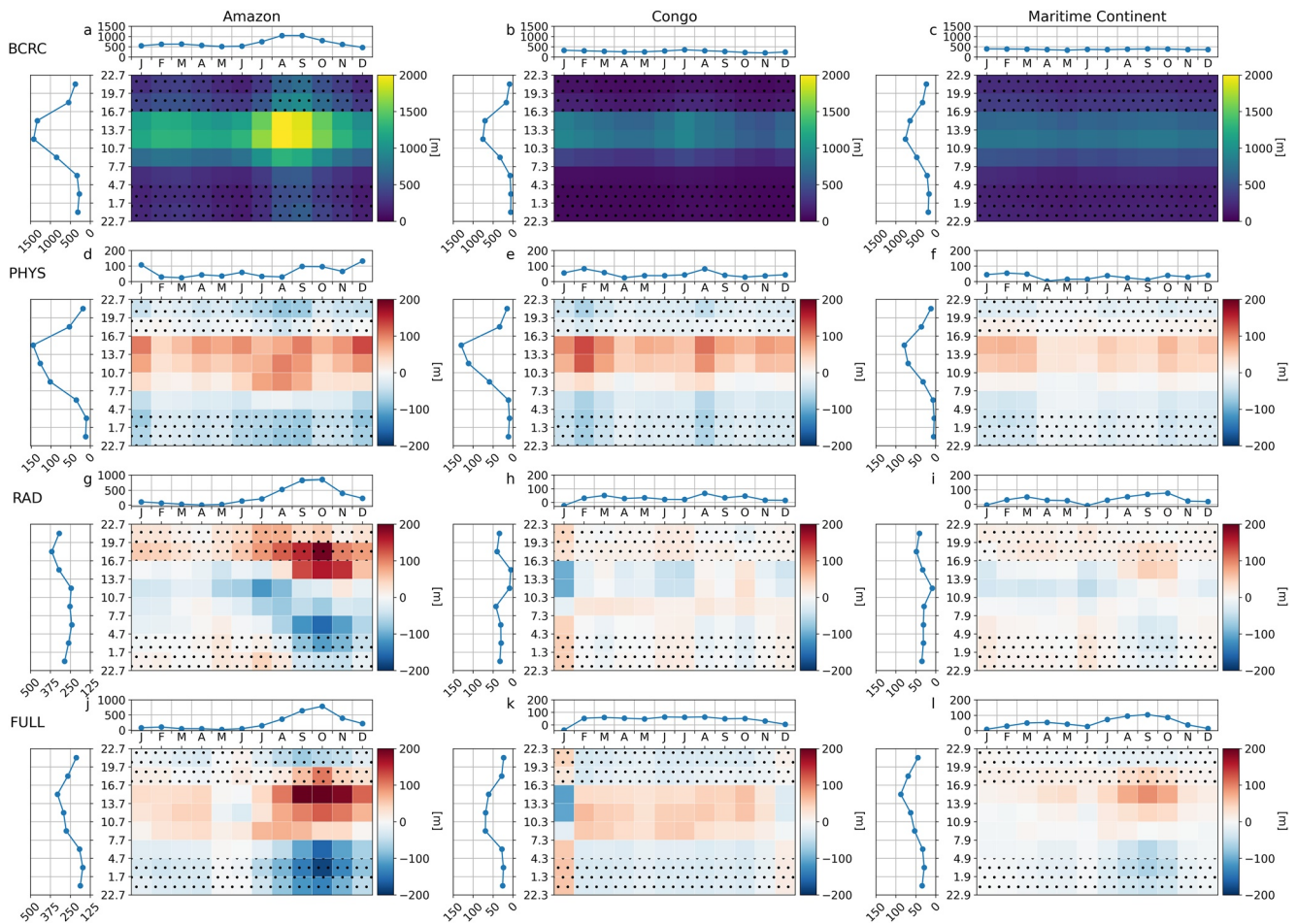


**Figure 11.** Diurnal and seasonal composite of lifting condensation level (LCL) height (BCRC; top row) and its changes owing to the physiological effect (BDRD – BCRC; second row), radiative effect (BCRD – BCRC; third row), and full effect (BDRD – BCRC; bottom row) for the Amazon (left column), Congo (middle column), and Maritime Continent (right column). The line plots to the top and left of each panel provide the daily mean seasonal variation and annual mean diurnal variation, respectively. All values are provided in units of m. Stippling indicates nighttime.

Continent than the Amazon and Congo, and the ET changes, which follow the diurnal cycle of solar radiation, do not show up as the primary factor influencing the reduction in precipitation diurnal cycle in our moisture budget analysis in Section 3. Despite these differences, the physical processes we have outlined in this section suggest that the transpiration reduction is influencing the boundary layer in the same way and is still the root cause of the rainfall reduction for all three tropical forest regions. The transpiration changes are likely also responsible for the phase delay from the physiological ET term in Figure 7. Our findings are consistent with prior work that has demonstrated a link between increasing LCL and a delay in convection (Chen et al., 2020; Louf et al., 2019).

Next, we seek to better understand why the radiative response also reduces rainfall diurnal amplitude. From Figures 6 and 8, there is not a consistent reduction in ET across the tropical forest regions, so there must be another factor at play. Figure 10 panels d–f show that the radiative responses for the deep convective water vapor tendency do not have the same dipole structure as the physiological response. Instead, the radiative response is characterized by a tripole structure that largely dampens the existing baseline structure. This suggests that convection is similar in both the BCRC and BCRD experiments, but there is simply less of it in the BCRD experiment. Figure 12 shows the frequency of deep convection in BCRC (top row) and its changes (second through fourth rows). Panels g–i show the radiative responses, and indeed there is a significant drop off in deep convective frequency that matches the timing in rainfall reduction. The reduction in frequency of the deep convective scheme from the radiative impact results from a reduction in Convective Available Potential Energy (CAPE; Figure 13) that occurs at the same time of day as the frequency reduction. In other words, as the climate warms,

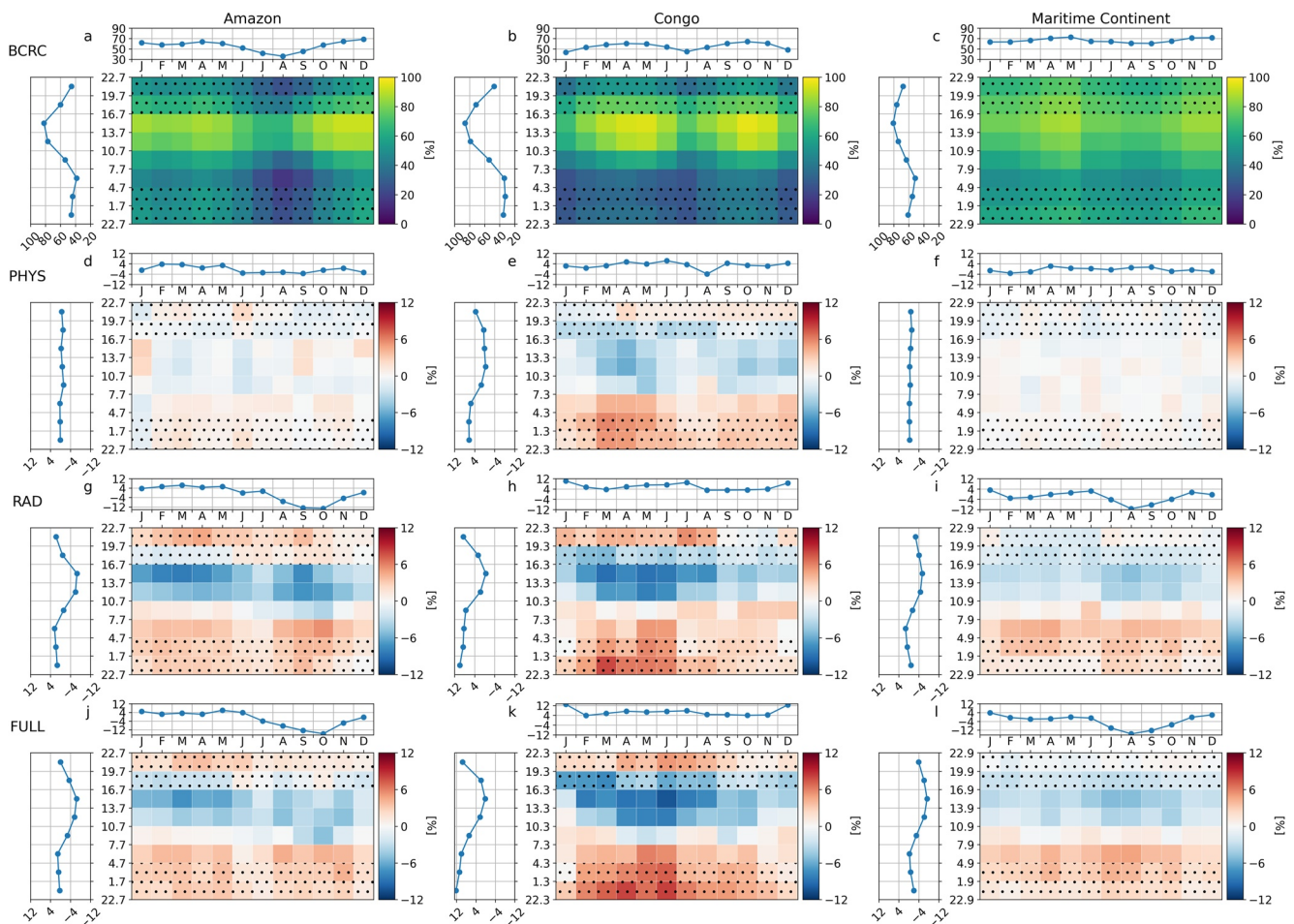


**Figure 12.** As in Figure 11 only for the frequency of the deep convective parameterization. All values are provided as percentages (top row) or changes in percent (second through fourth rows).

the atmosphere becomes slightly less favorable to daytime deep convection, which results in deep convection triggering less frequently and a reduction in diurnal rainfall amplitude over the tropical forest regions.

Figure 8 shows that the diurnal temperature radiative response has a minimum during the day. Nocturnal warming outpacing daytime warming is a well-established result of greenhouse gas warming (Karl et al., 1993; Easterling et al., 1997; New et al., 2000). Although not shown here, the near-surface equivalent potential temperature follows a similar pattern to the temperature response shown in Figure 8. Equivalent potential temperature values in the upper troposphere have a much smaller diurnal variation than the near-surface values (not shown), suggesting that it is the preference for warming to occur at night that makes daytime convection somewhat less favorable than nocturnal convection in these experiments. It is worth noting that averaged over the day, CAPE increases with radiative warming for these tropical forest regions (except over the Amazon during the dry season and wet season onset), in line with prior findings (Romps, 2016; Singh & O’Gorman, 2013). During the day, however, the change in CAPE is at its minimum. It is also worth noting that over the Congo region, CAPE and deep convective frequency increase at all hours, but their increase is weak during the day relative to the night, hence the dampening of the diurnal rainfall amplitude.

If one computes the change in precipitation expected from a drop off in deep convective frequency with the baseline rainfall (computed simply as the BCRC precipitation multiplied by the change in deep convective frequency between BCRD and BCRC), the change in rainfall is nearly identical to the changes in rainfall over the Congo and Maritime Continent. Over the Amazon, however, the reduction in deep convective frequency is insufficient to explain the rainfall reduction there (only accounting for about 25%–30% of the rainfall reduction shown in

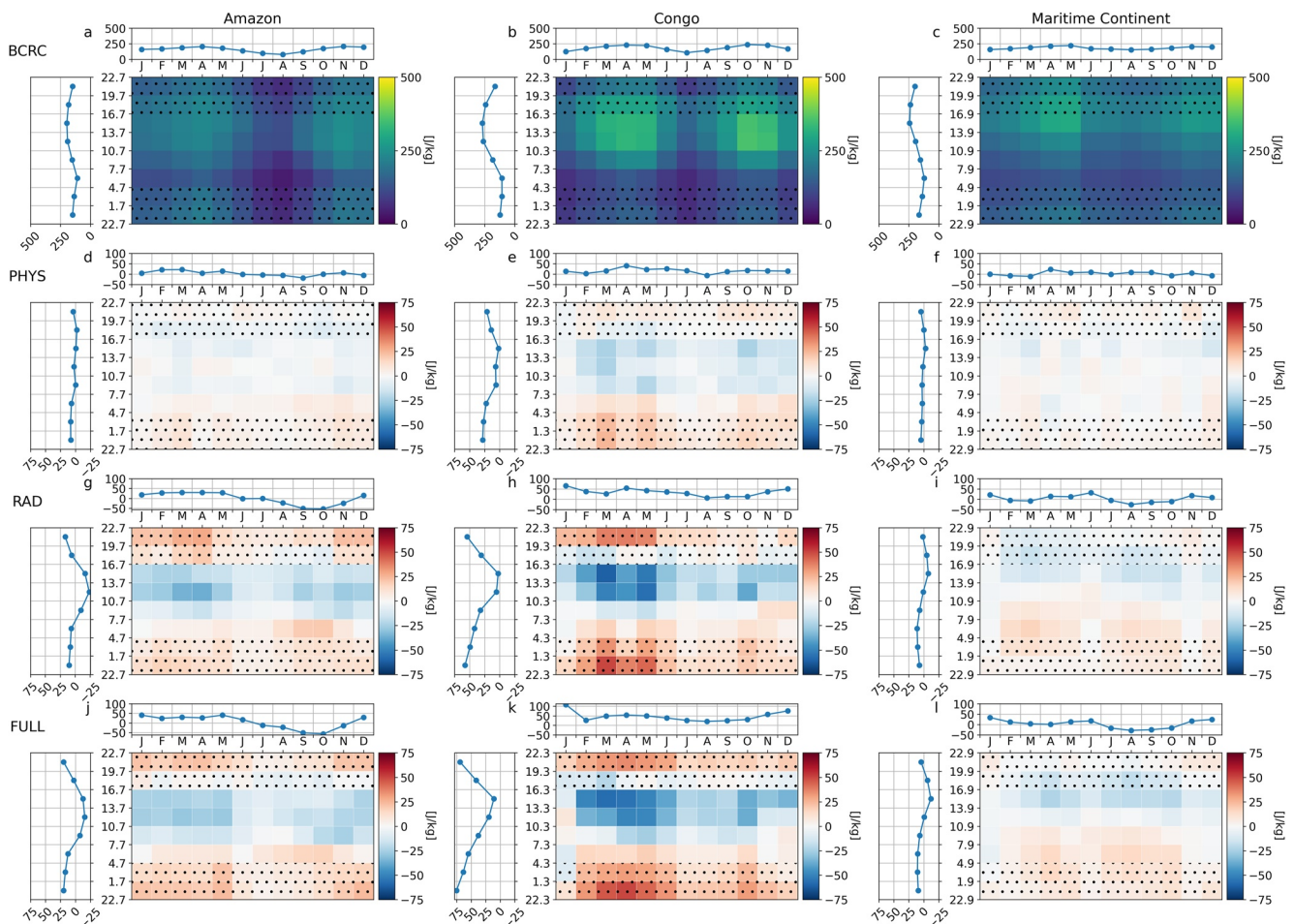


**Figure 13.** As in Figure 11 only for the Convective Available Potential Energy (CAPE). All values are provided in units of J/kg.

Figure 4). Figure 8 (third row) shows that the Amazon is the one region experiencing a large drop in transpiration. Following the same logic for the physiological response, there is an increase in LCL height resulting from the reduced transpiration, which is likely accounting for the additional reduction in rainfall (see Figure 11). Therefore, we can say that despite the physiological and radiative effects manifesting similar rainfall responses, the physical pathways that connect the responses with their drivers are different between the two. The full effect is mostly a superposition of the physiological and radiative effects (see Figures 6 and 10).

Finally, it is worth asking whether there is any change to rainfall extremes associated with the reduction in diurnal amplitude. An increased LCL has been linked to a delay of weak-to-moderate convection in favor of more intense convection later (Chen et al., 2020; Louf et al., 2019). As shown in Figure 7, there is an expected delay in the diurnal phase of rainfall from physiological ET changes (all else equal). Kooperman, Fowler, et al. (2018) showed that daily rainfall extremes have a weak increase in response to the physiological effect (weak compared to the radiative response), so it is worth revisiting this feature in case rainfall extremes on sub-daily timescales exhibit greater sensitivity to the physiological effect. To answer this question, we have examined the contribution of the 99th percentile to total rainfall for the three regions using years 2071–2100 (both CTC and ECA; see Figure 14). In the baseline, the fraction of rainfall coming from the 99th percentile is at its minimum when rainfall is at its maximum (at the end of the day). Similar to the weak increase in rainfall extremes found by Kooperman, Fowler, et al. (2018), the same response is found using the E3SMv1.1-BGC experiments. There is an increase in the fraction of rainfall coming from the 99th percentile, but like the results shown by Kooperman, Fowler, et al. (2018), the radiative response is significantly larger than that of the physiological response. It is worth noting that the physiological increase in the rainfall extreme fraction is largest at the end of the day, which is when the mean

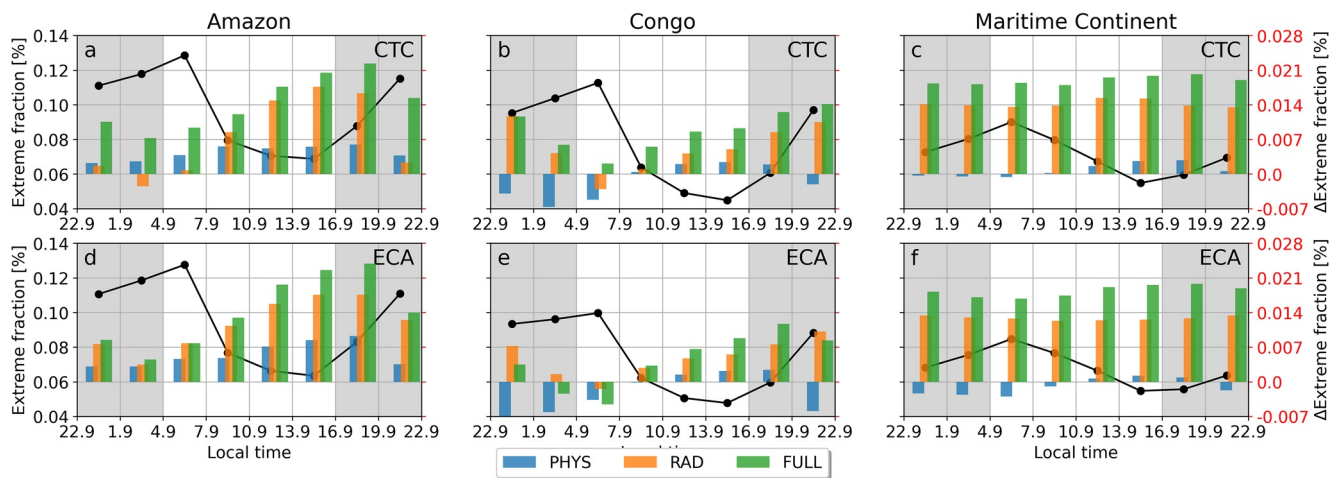


**Figure 14.** Fraction of rainfall coming from the 99th percentile in the baseline (black line) and its changes with respect to the physiological (BDRC – BCRC, blue), radiative (BCRD – BCRC, orange), and full (BDRD – BCRC, green) effects (colored bars). The top row shows results using the Converging Trophic Cascade (CTC) configuration and the bottom row shows results using the Equilibrium Chemistry Approximation (ECA) configuration.

rainfall decrease is largest. For the Congo and Maritime Continent basins, it is only during the end of the day that the rainfall extreme fraction increases at all, with decreases during the nighttime.

## 5. Summary and Conclusions

In this study we examined the tropical forest rainfall response to increasing  $\text{CO}_2$  in biogeochemistry-enabled E3SMv1.1 experiments. By compositing onto the diurnal and seasonal cycles, we found that both the physiological (BDRC – BCRC) and radiative (BCRD – BCRC) effects result in a reduction in the diurnal amplitude of rainfall for the three tropical forest regions examined here: the Amazon, Congo, and Maritime Continent. A moisture budget analysis revealed that the physiological effect is largely controlled by the reduction in surface evapotranspiration, while the radiative effect is largely controlled by changes in the moisture storage. The moisture budget analysis showed that the rainfall response to increasing  $\text{CO}_2$  is robust across different BGC configurations. As a result, only the CTC configuration was rerun for a 10 year segment to output additional 3-hourly output for analysis of the physical pathways connecting the physiological and radiative effects with their diurnal rainfall reductions.

Transpiration is the dominant component of the evapotranspiration (ET) over the tropical forest regions, and changes in transpiration account for most of the change in ET associated with the physiological effect. As atmospheric  $\text{CO}_2$  concentrations increase, stomatal closure reduces transpiration, which dries the boundary layer and raises the lifting condensation level, reducing the amount of rainfall occurring toward the end of the day, when the deep convective parameterization is most active. This finding agrees with similar findings from Langenbrunner et al. (2019), adding confidence to the conclusion. Like the findings of Kooperman, Fowler, et al. (2018) the increase in extreme rainfall from the physiological response is minor relative to the increase from the radiative and full responses.

The radiative effect follows a different physical pathway to connect increasing  $\text{CO}_2$  to reduced diurnal rainfall over the tropical forests. As the climate warms, the atmosphere becomes less favorable for deep convection during the day (seen as a minimum in CAPE change), which reduces the frequency of deep convection occurring over the tropical forests, and, ultimately, reduces rainfall during the time period where deep convection was most active in the baseline simulation. While there is likely some quantitative uncertainty associated with the specific deep convective parameterization used in the E3SM Atmosphere Model, the physical relationship between decreasing convective instability and decreasing rainfall should be present in any convective scheme, as well as convection-permitting simulations. The full effect is largely a superposition of the physiological and radiative effects. There is a reduction of diurnal rainfall with fingerprints of both the physiological effect reducing transpiration and elevating the LCL, as well as the warming reducing CAPE and the frequency of deep convection.

It was noted earlier that there is a well-documented bias in the diurnal phase of rainfall in E3SM compared to TRMM observations. The diurnal phase bias in E3SM is common to many other GCMs (Covey et al., 2016) and is present throughout the simulation (a similar bias is found for 1985–2014; not shown). While this deficit casts some doubt over the quantitative results of the moisture budget amplitude analysis owing to its dependence on the temporal alignment of the rainfall and surface fluxes, the physical pathways described in Section 4 are likely to impact rainfall in a similar fashion even if the diurnal phase bias is reduced in the model. These results may be worth revisiting in future versions of E3SM as some modifications have been underway to improve the diurnal cycle of precipitation in the model. Documenting the role of the diurnal rainfall phase alignment on future changes, as shown here, is a critical step for motivating improved representations of precipitation in conjunction with the physical pathways identified here. Xie et al. (2019) showed that changes in the convective triggering function for E3SM can lead to improvements in the diurnal cycle of precipitation over tropical forest areas. In particular, allowing the convective parcel to “launch” from model layers up to 600 hPa shifts the phase of rain over the Maritime Continent to closely match observations. Improvements to phase are smaller over the Amazon and Congo, and somewhat masked by an overall decrease in the amplitude of diurnal rainfall for these two basins compared to the control. Similarly, other model biases such as those in sea surface or land surface temperature could impact the quantitative response, but we still expect the qualitative response to remain.

One of the limitations of the experimental design is that the surface carbon exchange could not change the atmospheric CO<sub>2</sub> concentrations because the atmospheric CO<sub>2</sub> was prescribed in the E3SMv1.1-BGC simulations. Consequently, plants do not experience diurnal cycles in CO<sub>2</sub> within the atmospheric boundary layer, an interhemispheric gradient, or other spatiotemporal variations in CO<sub>2</sub>, which could potentially impact the strength of the stomatal response if CO<sub>2</sub> were simulated dynamically. Furthermore, important land surface processes such as plant hydraulics that influence the stomatal conductance and its response to CO<sub>2</sub> are not represented in E3SMv1.1-BGC. In the future, it will be valuable to revisit some of these findings when CO<sub>2</sub> is fully prognostic across all climate components and more land surface processes controlling ET are represented in the model.

The results suggest that the diurnal amplitude of rainfall over the tropical forests is likely to be reduced with increasing CO<sub>2</sub> concentrations. Both the physiological effect and radiative effect reduce the diurnal rainfall, though by different physical pathways. It is important to note that the change in the daily mean rainfall is not uniform across these three basins, it is simply the distribution of that rainfall within the diurnal cycle that is changing consistently. It is also worth noting that changing the relative balance between daytime and nocturnal rainfall could have important implications for other water cycle features. For example, the amount of rainwater that collects on the canopy and re-evaporates prior to reaching the ground may be reduced if rainfall preferentially occurs overnight when temperatures are cooler. While it was not the focus of this work, changes to rainfall timing may result in changes to shortwave cloud radiative effects and how much sunlight reaches the surface. Understanding the shortwave cloud response to the physiological effect requires understanding how cloud optical depth and amount change for deep convection as well as for shallower, potentially non-precipitating clouds. This work adds to a growing body of literature aiming to better understand the water cycle response of tropical forests to increasing atmospheric CO<sub>2</sub> concentrations.

### Appendix A: Additional Model Output From Reruns (2071–2080)

Three-hourly atmospheric data were output selectively for three regions encompassing the tropical forest regions used in this study: Amazon (265°E–315°E, 20°S–15°N); Congo (0°E–35°E, 10°S–10°N); Maritime Continent (85°E–180°E, 20°S–15°N). These data then used the same tropical forest masking criteria described in the manuscript to create the regional averages. Three-hourly land data were output globally. The three-hourly output fields exclusive to the reruns (not available from the original simulations) used in the analysis are listed below. (Table A1)

**Table A1**

*Extra Variables Used in This Study From the Rerun Segments of the Simulations*

Variable name	Atmosphere or land	2D or 3D	Variable description
CAPE	atmosphere	2D	Convective Available Potential Energy
FREQZM	atmosphere	2D	Frequency of deep convective triggering
PRECC	atmosphere	2D	“convective” precipitation (that formed by the deep convection parameterization)
PRECL	atmosphere	2D	“large-scale” precipitation (that formed by the microphysics parameterization)
Q	atmosphere	3D	Specific humidity
T	atmosphere	3D	Temperature
Z3	atmosphere	3D	Geopotential height
ZMDQ	atmosphere	3D	Deep convective moisture tendency
QSOIL	land	2D	Ground evaporation flux
QVEGE	land	2D	Canopy evaporation flux
QVEGT	land	2D	Canopy transpiration flux
TLAI	land	2D	Total projected leaf area index

*Note.* CAPE, Convective Available Potential Energy.

## Data Availability Statement

The processed output and script needed to generate the figures presented in this manuscript are archived at <https://doi.org/10.5281/zenodo.6330114>. NCO (Zender, 2008) was used to generate climatologies and for data regridding. Additional data processing made extensive use of the xarray python package for multi-dimensional arrays (Hoyer & Hamman, 2017).

## Acknowledgments

This research was supported as part of the Energy Exascale Earth System Model (E3SM) project, funded by the U.S. Department of Energy, Office of Science, Office of Biological and Environmental Research (BER), Earth System Model Development program area. The Pacific Northwest National Laboratory is operated for the U.S. DOE by Battelle Memorial Institute under contract DE-AC05-76RL01830. Part of the work was performed under the auspices of the U.S. Department of Energy by Lawrence Livermore National Laboratory under Contract DE-AC52-07NA27344. GJK acknowledges support from the U.S. Department of Energy BER Regional and Global Model Analysis (RGMA) Program (DE-SC0019459 and DE-SC0021209). The data were produced using resources of the National Energy Research Scientific Computing Center, a DOE Office of Science User Facility supported by the Office of Science of the U.S. Department of Energy under Contract No. DE-AC02-05CH11231.

## References

- Adams, M. A., Buckley, T. N., & Turnbull, T. L. (2020). Diminishing CO<sub>2</sub>-driven gains in water-use efficiency of global forests. *Nature Climate Change*, 10(5), 466–471. <https://doi.org/10.1038/s41558-020-0747-7>
- Bolton, D. (1980). The computation of equivalent potential temperature. *Monthly Weather Review*, 108(7), 1046–1053. [https://doi.org/10.1175/1520-0493\(1980\)108<1046:TCOEPT>2.0.CO;2](https://doi.org/10.1175/1520-0493(1980)108<1046:TCOEPT>2.0.CO;2)
- Burrows, S., Maltrud, M., Yang, X., Zhu, Q., Jeffery, N., Shi, X., et al. (2019). *Ilambv2.5 benchmarking results comparing e3smv1.1 cmip6 historical simulations with multi-model cmip5 historical simulations*. figshare. Retrieved from [https://figshare.com/articles/journal\\_contribution/ILAMBv2\\_5\\_benchmarking\\_results\\_comparing\\_E3SMv1\\_1\\_CMIP6\\_historical\\_simulations\\_with\\_multi-model\\_CMIP5\\_historical\\_simulations/11097356/2](https://figshare.com/articles/journal_contribution/ILAMBv2_5_benchmarking_results_comparing_E3SMv1_1_CMIP6_historical_simulations_with_multi-model_CMIP5_historical_simulations/11097356/2)
- Burrows, S. M., Maltrud, M., Yang, X., Zhu, Q., Jeffery, N., Shi, X., et al. (2020). The DOE E3SM v1.1 biogeochemistry configuration: Description and simulated ecosystem-climate responses to historical changes in forcing. *Journal of Advances in Modeling Earth Systems*, 1–59(9). <https://doi.org/10.1029/2019MS001766>
- Chadwick, R., Ackerley, D., Ogura, T., & Dommengat, D. (2019). Separating the Influences of land warming, the direct CO<sub>2</sub> effect, the plant physiological effect, and SST warming on regional precipitation changes. *Journal of Geophysical Research: Atmospheres*, 124(2), 624–640. <https://doi.org/10.1029/2018JD029423>
- Chadwick, R., Good, P., Andrews, T., & Martin, G. (2014). Surface warming patterns drive tropical rainfall pattern responses to CO<sub>2</sub> forcing on all timescales. *Geophysical Research Letters*, 41(2), 610–615. <https://doi.org/10.1002/2013GL058504>
- Chen, J., Dai, A., Zhang, Y., & Rasmussen, K. L. (2020). Changes in convective available potential energy and convective inhibition under global warming. *Journal of Climate*, 33(6), 2025–2050. <https://doi.org/10.1175/JCLI-D-19-0461.1>
- Cloke, H. L., & Pappenberger, F. (2009). Ensemble flood forecasting: A review. *Journal of Hydrology*, 375(3–4), 613–626. <https://doi.org/10.1016/j.jhydrol.2009.06.005>
- Collatz, G., Ball, J., Grivet, C., & Berry, J. A. (1991). Physiological and environmental regulation of stomatal conductance, photosynthesis and transpiration: A model that includes a laminar boundary layer. *Agricultural and Forest Meteorology*, 54(2), 107–136. [https://doi.org/10.1016/0168-1923\(91\)90002-8](https://doi.org/10.1016/0168-1923(91)90002-8)
- Collier, N., Hoffman, F. M., Lawrence, D. M., Keppel-Aleks, G., Koven, C. D., Riley, W. J., et al. (2018). The International Land Model Benchmarking (ILAMB) System: Design, theory, and Implementation. *Journal of Advances in Modeling Earth Systems*, 10(11), 2731–2754. <https://doi.org/10.1029/2018MS001354>
- Cook, K. H., Hsieh, J.-S., & Hagos, S. M. (2004). The Africa–South America intercontinental teleconnection. *Journal of Climate*, 17(14), 2851–2865. [https://doi.org/10.1175/1520-0442\(2004\)017<2851:TAAIT>2.0.CO;2](https://doi.org/10.1175/1520-0442(2004)017<2851:TAAIT>2.0.CO;2)
- Covey, C., Gleckler, P. J., Doutriaux, C., Williams, D. N., Dai, A., Fasullo, J., et al. (2016). Metrics for the diurnal cycle of precipitation: Toward routine benchmarks for climate models. *Journal of Climate*, 29(12), 4461–4471. <https://doi.org/10.1175/JCLI-D-15-0664.1>
- Creese, A., Washington, R., & Munday, C. (2019). The plausibility of September–November Congo basin rainfall change in coupled climate models. *Journal of Geophysical Research: Atmospheres*, 124(11), 5822–5846. <https://doi.org/10.1029/2018JD029847>

- Dai, A., & Trenberth, K. E. (2004). The diurnal cycle and its depiction in the community climate system model. *Journal of Climate*, 17(5), 930–951. [https://doi.org/10.1175/1520-0442\(2004\)017<0930:tdcaid>2.0.co;2](https://doi.org/10.1175/1520-0442(2004)017<0930:tdcaid>2.0.co;2)
- Dai, A., Trenberth, K. E., & Karl, T. R. (1999). Effects of clouds, soil moisture, precipitation, and water vapor on diurnal temperature range. *Journal of Climate*, 12(82), 2451–2473. [https://doi.org/10.1175/1520-0442\(1999\)012<2451:eocsmv>2.0.co;2](https://doi.org/10.1175/1520-0442(1999)012<2451:eocsmv>2.0.co;2)
- De Kauwe, M. G., Disney, M. I., Quaife, T., Lewis, P., & Williams, M. (2011). An assessment of the MODIS collection 5 leaf area index product for a region of mixed coniferous forest. *Remote Sensing of Environment*, 115(2), 767–780. <https://doi.org/10.1016/j.rse.2010.11.004>
- Easterling, D. R., Horton, B., Jones, P. D., Peterson, T. C., Karl, T. R., Parker, D. E., et al. (1997). Maximum and minimum temperature trends for the globe. *Science*, 277(5324), 364–367. <https://doi.org/10.1126/science.277.5324.364>
- Fiedler, S., Crueger, T., D'Agostino, R., Peters, K., Becker, T., Leutwyler, D., et al. (2020). Simulated tropical precipitation assessed across three major phases of the coupled model intercomparison project (CMIP). *Monthly Weather Review*, 148(9), 3653–3680. <https://doi.org/10.1175/MWR-D-19-0404.1>
- Field, C. B., Jackson, R. B., & Mooney, H. A. (1995). Stomatal responses to increased CO<sub>2</sub>: Implications from the plant to the global scale. *Plant, Cell and Environment*, 18(10), 1214–1225. <https://doi.org/10.1111/j.1365-3040.1995.tb00630.x>
- Fleischer, K., Rammig, A., De Kauwe, M., Walker, A., Domingues, T., Fuchslueger, L., et al. (2019). Amazon forest response to CO<sub>2</sub> fertilization depend on plant phosphorus acquisition. *Nature Geoscience*. (accepted). <https://doi.org/10.1038/s41561-019-0404-9>
- Fowler, M. D., Kooperman, G. J., Randerson, J. T., & Pritchard, M. S. (2019). The effect of plant physiological responses to rising CO<sub>2</sub> on global streamflow. *Nature Climate Change*, 9(11), 873–879. <https://doi.org/10.1038/s41558-019-0602-x>
- Garcia, B. N., Libonati, R., & Nunes, A. M. (2018). Extreme drought events over the Amazon Basin: The perspective from the reconstruction of South American Hydroclimate. *Water*, 10(11), 1594. <https://doi.org/10.3390/w10111594>
- Golaz, J., Caldwell, P. M., Van Roekel, L. P., Petersen, M. R., Tang, Q., Wolfe, J. D., et al. (2019). The DOE E3SM coupled model version 1: Overview and evaluation at standard resolution. *Journal of Advances in Modeling Earth Systems*, 11(7), 2089–2129. <https://doi.org/10.1029/2018ms001603>
- Hoegh-Guldberg, O., Jacob, D., Taylor, M., Guillén Bolaños, T., Bindi, M., Brown, S., et al. (2019). The human imperative of stabilizing global climate change at 1.5°C. *Science*, 365(6459). <https://doi.org/10.1126/science.aaw6974>
- Hoyer, S., & Hamman, J. J. (2017). xarray: N-D labeled arrays and datasets in Python. *Journal of Open Research Software*, 5, 1–6. <https://doi.org/10.5334/jors.148>
- Huffman, G. J., Adler, R. F., Bolvin, D. T., Gu, G., Nelkin, E. J., Bowman, K. P., et al. (2007). The TRMM multisatellite precipitation analysis (TMPA): Quasi-global, multiyear, combined-sensor precipitation estimates at fine scales. *Journal of Hydrometeorology*, 8(1), 38–55. <https://doi.org/10.1175/JHM560.1>
- Jones, C. D., Arora, V., Friedlingstein, P., Bopp, L., Brovkin, V., Dunne, J., et al. (2016). C4MIP-The coupled climate-carbon cycle model intercomparison project: Experimental protocol for CMIP6. *Geoscientific Model Development*, 9(8), 2853–2880. <https://doi.org/10.5194/gmd-9-2853-2016>
- Jung, M., Reichstein, M., Ciais, P., Seneviratne, S. I., Sheffield, J., Goulden, M. L., et al. (2010). Recent decline in the global land evapotranspiration trend due to limited moisture supply. *Nature*, 467(7318), 951–954. <https://doi.org/10.1038/nature09396>
- Karl, T. R., Jones, P. D., Gallo, K. P., Knight, R. W., Kukla, G., Plummer, N., et al. (1993). A new perspective on recent global warming: Asymmetric trends of daily maximum and minimum temperature articles reporting on the U.S. global change research program and international global change activities with and the human dimensions of global e. *Bulletin of the American Meteorological Society*, 74(6), 1007–1024. [https://doi.org/10.1175/1520-0477\(1993\)074<1007:anporg>2.0.co;2](https://doi.org/10.1175/1520-0477(1993)074<1007:anporg>2.0.co;2)
- Kooperman, G. J., Chen, Y., Hoffman, F. M., Koven, C. D., Lindsay, K., Pritchard, M. S., et al. (2018). Forest response to rising CO<sub>2</sub> drives zonally asymmetric rainfall change over tropical land. *Nature Climate Change*, 8(5), 434–440. <https://doi.org/10.1038/s41558-018-0144-7>
- Kooperman, G. J., Fowler, M. D., Hoffman, F. M., Koven, C. D., Lindsay, K., Pritchard, M. S., et al. (2018). Plant Physiological Responses to Rising CO<sub>2</sub> Modify Simulated Daily Runoff Intensity With Implications for Global-Scale Flood Risk Assessment. *Geophysical Research Letters*, 45(22), 12457–12466. <https://doi.org/10.1029/2018GL079901>
- Langenbrunner, B., Pritchard, M. S., Kooperman, G. J., & Randerson, J. T. (2019). Why Does Amazon Precipitation Decrease When tropical Forests Respond to Increasing CO<sub>2</sub>? *Earth's Future*, 7(4), 450–468. <https://doi.org/10.1029/2018EF001026>
- Lawrence, D. M., Thornton, P. E., Oleson, K. W., & Bonan, G. B. (2007). The partitioning of evapotranspiration into transpiration, soil evaporation, and canopy evaporation in a GCM: Impacts on land-atmosphere interaction. *Journal of Hydrometeorology*, 8(4), 862–880. <https://doi.org/10.1175/JHM596.1>
- Lawrence, P. J., & Chase, T. N. (2007). Representing a new MODIS consistent land surface in the Community Land Model (CLM 3.0). *Journal of Geophysical Research*, 112(1), G01023. <https://doi.org/10.1029/2006JG000168>
- Lian, X., Piao, S., Huntingford, C., Li, Y., Zeng, Z., Wang, X., et al. (2018). Partitioning global land evapotranspiration using CMIP5 models constrained by observations. *Nature Climate Change*, 8(7), 640–646. <https://doi.org/10.1038/s41558-018-0207-9>
- Louf, V., Jakob, C., Protat, A., Bergemann, M., & Narsey, S. (2019). The relationship of cloud number and size with their large-scale environment in deep tropical convection. *Geophysical Research Letters*, 46(15), 9203–9212. <https://doi.org/10.1029/2019GL083964>
- Markham, C. G. (1970). Seasonality of precipitation in the United States. *Annals of the Association of American Geographers*, 60(3), 593–597. <https://doi.org/10.1111/j.1467-8306.1970.tb00743.x>
- Meredith, E. P., Ulbrich, U., Rust, H. W., & Truhetz, H. (2021). Present and future diurnal hourly precipitation in 0.11°EURO-CORDEX models and at convection-permitting resolution. *Environmental Research Communications*, 3(5), 055002. <https://doi.org/10.1088/2515-7620/abf15e>
- Miralles, D. G., Holmes, T. R., De Jeu, R. A., Gash, J. H., Meesters, A. G., & Dolman, A. J. (2011). Global land-surface evaporation estimated from satellite-based observations. *Hydrology and Earth System Sciences*, 15(2), 453–469. <https://doi.org/10.5194/hess-15-453-2011>
- Neale, R. B., Richter, J. H., & Jochum, M. (2008). The impact of convection on ENSO: From a delayed oscillator to a series of events. *Journal of Climate*, 21(22), 5904–5924. <https://doi.org/10.1175/2008JCLI2244.1>
- New, M., Hulme, M., & Jones, P. (2000). Representing twentieth-century space-time climate variability. Part II: Development of 1901–96 monthly grids of terrestrial surface climate. *Journal of Climate*, 13(13), 2217–2238. [https://doi.org/10.1175/1520-0442\(2000\)013<2217:RTCSTC>2.0.CO;2](https://doi.org/10.1175/1520-0442(2000)013<2217:RTCSTC>2.0.CO;2)
- Oleson, K. W., Lawrence, D. M., Bonan, G. B., Drewniak, B., Huang, M., Koven, C. D., et al. (2013). *Technical description of version 4.5 of the Community Land Model (CLM)*. NCAR/TN-478+STR NCAR Technical Note(April). <https://doi.org/10.5065/D6RR1W7M>
- O'Neill, B. C., Tebaldi, C., Van Vuuren, D. P., Eyring, V., Friedlingstein, P., Hurtt, G., et al. (2016). The scenario model intercomparison project (ScenarioMIP) for CMIP6. *Geoscientific Model Development*, 9(9), 3461–3482. <https://doi.org/10.5194/gmd-9-3461-2016>
- Ozdogan, M., Yang, Y., Allez, G., & Cervantes, C. (2010). Remote sensing of irrigated agriculture: Opportunities and challenges. *Remote Sensing*, 2(9), 2274–2304. <https://doi.org/10.3390/rs2092274>

- Pietschnig, M., Lambert, F. H., Saint-Lu, M., & Vallis, G. K. (2019). The presence of Africa and limited soil moisture contribute to future drying of South America. *Geophysical Research Letters*, *46*(21), 12445–12453. <https://doi.org/10.1029/2019GL084441>
- Rasch, P. J., Xie, S., Ma, P. L., Lin, W., Wang, H., Tang, Q., et al. (2019). An overview of the atmospheric component of the Energy Exascale Earth System Model. *Journal of Advances in Modeling Earth Systems*, *11*(8), 2377–2411. <https://doi.org/10.1029/2019MS001629>
- Reboita, M. S., Dutra, L. M. M., & Dias, C. G. (2016). Diurnal cycle of precipitation simulated by RegCM4 over South America: Present and future scenarios. *Climate Research*, *70*(1), 39–55. <https://doi.org/10.3354/cr01416>
- Richter, J. H., & Rasch, P. J. (2008). Effects of convective momentum transport on the atmospheric circulation in the Community Atmosphere Model, Version 3. *Journal of Climate*, *21*(7), 1487–1499. <https://doi.org/10.1175/2007JCLI1789.1>
- Romps, D. M. (2016). Clausius–Clapeyron scaling of CAPE from analytical solutions to RCE. *Journal of the Atmospheric Sciences*, *73*(9), 3719–3737. <https://doi.org/10.1175/JAS-D-15-0327.1>
- Saint-Lu, M., Chadwick, R., Lambert, F. H., & Collins, M. (2019). Surface warming and atmospheric circulation dominate rainfall changes over tropical rainforests under global warming. *Geophysical Research Letters*, *46*(22), 13410–13419. <https://doi.org/10.1029/2019GL085295>
- Scaff, L., Prein, A. F., Li, Y., Liu, C., Rasmussen, R., & Ikeda, K. (2020). Simulating the convective precipitation diurnal cycle in North America's current and future climate. *Climate Dynamics*, *55*(1–2), 369–382. <https://doi.org/10.1007/s00382-019-04754-9>
- Sellers, P., Randall, D., Collatz, G., Berry, J., Field, C., Dazlich, D., et al. (1996). A revised land surface parameterization (SiB2) for atmospheric GCMs. Part I: Model Formulation. *Journal of Climate*, *9*(4), 676–705. [https://doi.org/10.1175/1520-0442\(1996\)009<0676:ARLSPF>2.0.CO;2](https://doi.org/10.1175/1520-0442(1996)009<0676:ARLSPF>2.0.CO;2)
- Singh, M. S., & O'Gorman, P. A. (2013). Influence of entrainment on the thermal stratification in simulations of radiative-convective equilibrium. *Geophysical Research Letters*, *40*(16), 4398–4403. <https://doi.org/10.1002/grl.50796>
- Song, F., Leung, L. R., Lu, J., & Dong, L. (2018a). Future changes in seasonality of the North Pacific and North Atlantic subtropical highs. *Geophysical Research Letters*, *45*(21), 11959–11968. <https://doi.org/10.1029/2018GL079940>
- Song, F., Leung, L. R., Lu, J., & Dong, L. (2018b). Seasonally dependent responses of subtropical highs and tropical rainfall to anthropogenic warming. *Nature Climate Change*, *8*(9), 787–792. <https://doi.org/10.1038/s41558-018-0244-4>
- Song, F., Leung, L. R., Lu, J., Dong, L., Zhou, W., Harrop, B., & Qian, Y. (2021). Emergence of seasonal delay of tropical rainfall during 1979–2019. *Nature Climate Change*, *11*(7), 605–612. <https://doi.org/10.1038/s41558-021-01066-x>
- Spracklen, D. V., Baker, J. C., Garcia-Carreras, L., & Marsham, J. H. (2018). The effects of tropical vegetation on rainfall. *Annual Review of Environment and Resources*, *43*(1), 193–218. <https://doi.org/10.1146/annurev-environ-102017-030136>
- Swann, A. L. S., Hoffman, F. M., Koven, C. D., & Randerson, J. T. (2016). Plant responses to increasing CO2 reduce estimates of climate impacts on drought severity. *Proceedings of the National Academy of Sciences*, *113*(36), 10019–10024. <https://doi.org/10.1073/pnas.1604581113>
- Thornton, P., Law, B., Gholz, H. L., Clark, K. L., Falge, E., Ellsworth, D., et al. (2002). Modeling and measuring the effects of disturbance history and climate on carbon and water budgets in evergreen needleleaf forests. *Agricultural and Forest Meteorology*, *113*(1–4), 185–222. [https://doi.org/10.1016/S0168-1923\(02\)00108-9](https://doi.org/10.1016/S0168-1923(02)00108-9)
- Thornton, P. E., & Rosenbloom, N. A. (2005). Ecosystem model spin-up: Estimating steady state conditions in a coupled terrestrial carbon and nitrogen cycle model. *Ecological Modelling*, *189*(1–2), 25–48. <https://doi.org/10.1016/j.ecolmodel.2005.04.008>
- Vicente-Serrano, S. M., Quiring, S. M., Peña-Gallardo, M., Yuan, S., & Domínguez-Castro, F. (2020). A review of environmental droughts: Increased risk under global warming? *Earth-Science Reviews*, *201*, 102953. <https://doi.org/10.1016/j.earscirev.2019.102953>
- Vilà-Guerau de Arellano, J., Wang, X., Pedruzo-Bagazgoitia, X., Sikma, M., Agusti-Panareda, A., Boussetta, S., et al. (2020). Interactions between the Amazonian rainforest and cumuli clouds: A large-eddy simulation, high-resolution ECMWF and observational intercomparison study. *Journal of Advances in Modeling Earth Systems*, *12*(7), 1–33. <https://doi.org/10.1029/2019ms001828>
- Westerling, A. L., Gershunov, A., Brown, T. J., Cayan, D. R., & Dettinger, M. D. (2003). Climate and wildfire in the western United States. *Bulletin of the American Meteorological Society*, *84*(5), 595–604+548. <https://doi.org/10.1175/BAMS-84-5-595>
- Xie, S., Wang, Y.-C., Lin, W., Ma, H.-Y., Tang, Q., Tang, S., et al. (2019). Improved diurnal cycle of precipitation in E3SM with a revised convective triggering function. *Journal of Advances in Modeling Earth Systems*, *11*(7), 2290–2310. <https://doi.org/10.1029/2019MS001702>
- Zender, C. S. (2008). Analysis of self-describing gridded geoscience data with netCDF Operators (NCO). *Environmental Modelling & Software*, *23*(10), 1338–1342. <https://doi.org/10.1016/j.envsoft.2008.03.004>
- Zhang, G. J., & McFarlane, N. A. (1995). Sensitivity of climate simulations to the parameterization of cumulus convection in the Canadian climate centre general circulation model. *Atmosphere-Ocean*, *33*(3), 407–446. <https://doi.org/10.1080/07055900.1995.9649539>
- Zhu, Q., Riley, W. J., Iversen, C. M., & Kattge, J. (2020). Assessing impacts of plant stoichiometric traits on terrestrial ecosystem carbon accumulation using the E3SM land model. *Journal of Advances in Modeling Earth Systems*, *12*(4). <https://doi.org/10.1029/2019MS001841>
- Zhu, Q., Riley, W. J., Tang, J., Collier, N., Hoffman, F. M., Yang, X., & Bisht, G. (2019). Representing nitrogen, phosphorus, and carbon interactions in the E3SM Land Model: Development and global benchmarking. *Journal of Advances in Modeling Earth Systems*, *11*(7), 2238–2258. <https://doi.org/10.1029/2018MS001571>
- Zhu, Q., Riley, W. J., Tang, J., & Koven, C. D. (2016). Multiple soil nutrient competition between plants, microbes, and mineral surfaces: Model development, parameterization, and example applications in several tropical forests. *Biogeosciences*, *13*(1), 341–363. <https://doi.org/10.5194/bg-13-341-2016>